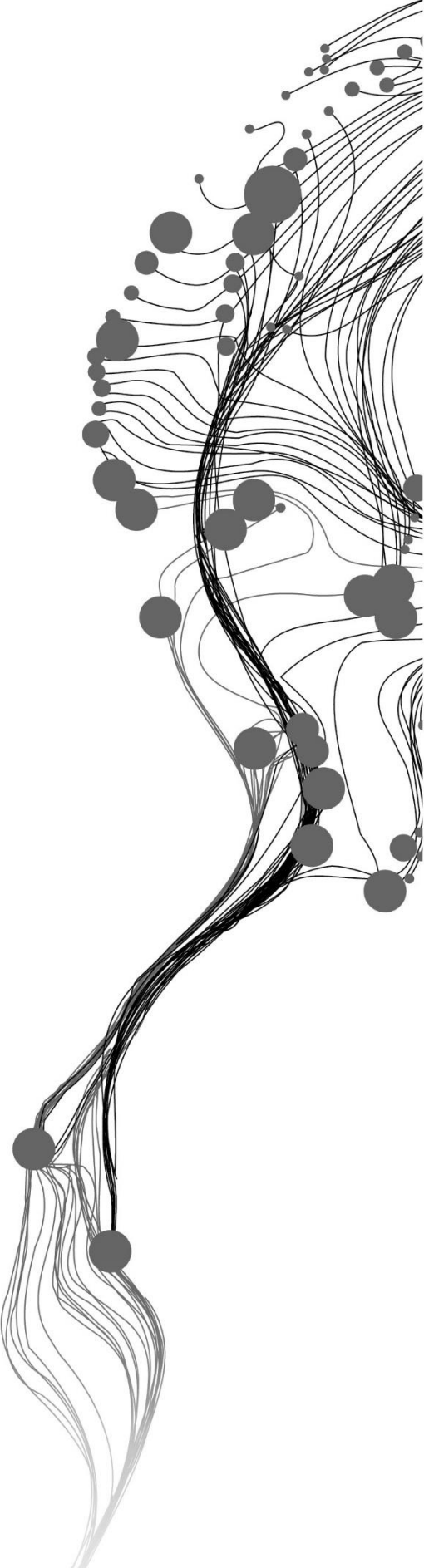


Hydrogeophysics for designing the hydrogeophysical conceptual model of a sub-catchment in Maqu, Tibet-China

Janvier Uwiringiyimana
February 2019

SUPERVISORS:
Dr. Yijian Zeng
Dr. MACIEK.W. Lubczynski

ADVISOR:
Mengna Li



Hydrogeophysics for designing the hydrogeophysical conceptual model of a sub-catchment in Maqu, Tibet-China

Janvier Uwiringiyimana

Enschede, The Netherlands, February 2019

Thesis submitted to the Faculty of Geo-Information Science and Earth Observation of the University of Twente in partial fulfilment of the requirements for the degree of Master of Science in Geo-information Science and Earth Observation.

Specialization: Water Resources and Environmental Management

SUPERVISORS:

Dr. Yijian Zeng

Dr. M.W. Lubczynski

ADVISOR:

Mengna Li

THESIS ASSESSMENT BOARD:

Prof. dr. Z Su (Chair)

Dr. P. Gurwin (External Examiner , University of Wraclow, Poland)

DISCLAIMER

This document describes work undertaken as part of a programme of study at the Faculty of Geo-Information Science and Earth Observation of the University of Twente. All views and opinions expressed therein remain the sole responsibility of the author and do not necessarily represent those of the Faculty.

Abstract

Maqu sub-catchment is located on the eastern edge of Tibetan Plateau in China, the upper part of the Yellow River basin. This river section is considered as a source of Yellow River. In response to climate change on Tibetan Plateau, elements of the hydrological cycle have been affected, which resulted in uncertainties for river discharge trends over the basins. Maqu sub-catchment is not an exception, due to climate warming, the maximum depth of snow has decreased, and thickness of the active layer has increased in frozen ground. The River baseflow, groundwater flow, streamflow, and surface runoff are reported to exhibit a strong decreasing trend mainly in the course of Yellow River runoff production. Therefore, there is a need to understand the impact of the subsurface hydrogeological setting on groundwater occurrence and its influence on streamflow dynamics at catchment scale. This is particularly true over Tibetan Plateau, as most of the studies have been focused on streamflow climatology and its relation to precipitations and temperature changes but not much on groundwater-related perspective.

This thesis demonstrates the integral application of two hydrogeophysical methods such as Magnetic Resonance Sounding (MRS) and two-dimensional Electrical Resistivity Tomography (2D ERT) to characterize the subsurface hydrogeological setting. Particularly, the 3D modeling software (RockWorks) was applied to provide the spatial extent of hydrogeophysical layers, which can be used as a step forward for the analysis of groundwater dynamic. After the interpretation of hydrogeophysical parameters, it was found that the study area can be divided into two components. One component with topographic relief that acts as water collector and a plain component with storage role. In general, three depth-wise hydrogeophysical layers were estimated for the plain component: i) a thin surficial layer with high electrical resistivity $>200\Omega.m$ and low average MRS water content $\sim 3.6\%$, which is referred as unsaturated zone whose granulometry composed by very fine sands and clay sands; ii) the second layer with high MRS water content $\sim 16.9\%$ and less developed electrical resistivity $<150\ \Omega.m$, which is interpreted as a saturated zone with granulometry composed by a mixture of fine sands and coarse gravels as revealed by MRS decay time constant; and iii) the third layer – a thick deep layer up to the depth of investigation with low average of MRS water content $\sim 2.49\%$ and increased electrical resistivity $>150\ \Omega.m$, which is interpreted as saturated zone but with less storage composed by some form of consolidated sediments with less porosity. The MRS hydraulic conductivity for saturated layer was calculated using the calibration coefficient assigned for the layers with similar lithological properties as found in the literature. The estimated value varies between $0.04\ m\ d^{-1}$ to $1.1\ m.d^{-1}$ for fine sands to coarse gravels respectively. The MRS specific yield was estimated using a graph relating MRS water content to the specific yield and the average value of 5.4% was estimated.

Keywords: Hydrogeophysical methods; Hydrogeophysical model; MRS Hydraulic parameters; RockWorks; Tibetan Plateau

Acknowledgments

First of all , I am grateful to the almighty God for blessing and good health all along the journey. Secondly, I would like to express my sincere gratitude to the government of the Netherlands through NFP for providing me a scholarship to study in a multicultural environment.

I also wish to express my deep sense of gratitude to my Supervisors Dr.Yijian Zeng and Dr. M.W. Lubczynski for the valuable and inspiring guidance and constant encouragement in preparation of this Manuscript. I am extremely grateful to My Advisor, Ms. Mengna Li who has always been available for suggestions and kind help all along this work. I would also like to extend my sincere gratitude to Dr.Jean Roy for advice and valuable comments, thank you very much.

I extend my sincere appreciations to all members of the Faculty of Geo-Information Science and Earth Observation of the University of Twente for providing a sense of community. I also express my heartfelt thanks to my Father, brothers and sisters, loving family members, fellow students, and friends who have directly and indirectly supported me in all needful times; God bless you

TABLE OF CONTENTS

1.	Introduction.....	1
1.1.	Background to subsurface hydrogeological modeling	1
1.2.	Problem description.....	2
1.3.	Assumption.....	2
1.4.	Research objectives	2
1.5.	Research questions	3
1.6.	Characteristics of the study area	3
1.6.1.	Location.....	3
1.6.2.	Climate.....	4
1.6.3.	Hydrology.....	4
1.6.4.	Geological setting.....	4
2.	Previous hydrological studies in the study area.....	5
3.	Hydrogeological characterization with geophysical methods.....	6
3.1.	Electrical Resistivity Tomography (ERT)	7
3.1.1.	Introduction to resistivity measurement	7
3.1.2.	Resistivity measurement procedure with 2D Survey.....	9
3.1.3.	Data processing and presentation	11
3.2.	Magnetic Resonance Sounding (MRS)	12
3.2.1.	Background and field measurement procedures.....	12
3.2.2.	Data inversion	14
3.2.3.	Hydrogeological parameterization with MRS.....	15
4.	Three-Dimensional hydrogeological modelling.....	20
5.	Methodology.....	21
5.1.	Data Sources and formats.....	22
5.1.1.	Digital Elevation Models (DEM)	22
5.1.2.	Geophysical datasets.....	22
5.1.3.	Existing borehole logging.....	23
5.2.	Data preparation	25
5.2.1.	ERT data processing	25
5.2.2.	MRS data set	29
5.2.3.	Model extent and digital elevation model	30
5.3.	Software consideration	31
5.4.	Three-dimensional modeling and database structure.....	31
6.	Results and discussion.....	33
6.1.	2D ERT inversion results	33
6.2.	Comparison of MRS and ERT outputs.....	34
6.3.	Subsurface hydrogeophysical characterization.....	39
6.3.1.	3-D Resistivity modeling and interpretation.....	39
6.3.2.	Insight into subsurface hydrogeological setting based on MRS outputs	41
6.3.3.	Hydrogeophysical interpretation with applied geophysical methods	50
7.	Conclusion and Recommendation.....	52
7.1.	Conclusion.....	52
7.2.	Recommendations	52
	List of references	54

Appendices57

LIST OF FIGURES

Figure 1. Location of the study area (elevation data are provided by USGS SRTM 30)	3
Figure 2 . Simplified geological map of the study area	5
Figure 3. The arrangement of electrodes for a 2 D ERT survey and the sequence of measurement used to build up a pseudo section (from Loke 2004).	10
Figure 4. General principle and configuration of MRS : 1: Antenna, 2: promotion of energy generated by the device Tx (3), 4: MRS signal generated by hydrogen protons and taken by the device (from Bernard et al. 2006).	13
Figure 5. MRS signal amplitude curve for different aquifers, various types of thickness and depths(from Bernard et al. 2006).	14
Figure 6. Aquifer groundwater storage concept (after Lubczynski and Roy 2003)	16
Figure 7. A model relating total porosity, specific yield, specific retention, MRS water content and undetectable water by MRS as a function of grain size and corresponding diagram of the MRS water content as function specific yield (Adapted from Boucher et al. 2009).....	18
Figure 8. Types of modeling methods according to the type of data available and from which domain they originate (from Natali et al. 2013)	20
Figure 9. Methodology Flow chart diagram.....	21
Figure 10. Field plan and location of ERT Lines, MRS detection loop.	23
Figure 11. Existing borehole logging.....	24
Figure 12. Example of data scatter before noise data rejection	26
Figure 13. Example of Screenshot for inversion results with Res2dinv software.....	27
Figure 14. 2D Resistivity processing flowchart	28
Figure 15. Data removal filter during pre-inversion process (ERT Line 2, Wenner array configuration).....	28
Figure 16. An overview of modeling extent with a location of geophysical survey and existing well logging	30
Figure 17. Model extent: 3-D Digital elevation model	31
Figure 18. a) ERT Line1 Wenner configuration, b) ERT Line1 Dipole Dipole Configuration, C) MRS 8-2: Water content and T2* versus depth.....	35
Figure 19 a) ERT Line2 Wenner configuration, b) ERT Line2 Dipole-Dipole Configuration, C) MRS 2-1: Water content (%) and T2* versus depth	35
Figure 20 a)ERT Line3 Wenner configuration, b) ERT Line3 Dipole Dipole Configuration, C) MRS 3-2: Water content (%) and T2* versus depth.	36
Figure 21 a)ERT Line4 Wenner configuration, b) ERT Line4 Dipole Dipole Configuration, C) MRS 5-2: Water content (%) and T2* versus depth.	36
Figure 22 a)ERT Line5 Wenner configuration, b) ERT Line5 Dipole Dipole Configuration, C) MRS 8-1: Water content (%) and T2* versus depth.	37
Figure 23 a) ERT Line6 Wenner configuration, b) ERT Line6 Dipole Dipole Configuration, C) MRS 7-2: Water content (%) and T2* versus depth.	37
Figure 24 a) ERT Line7 Wenner configuration, b) ERT Line5 Dipole Dipole Configuration, C) MRS 8-1: Water content (%) and T2* versus depth.	38
Figure 25. Frequency distribution of 2D resistivity (true resistivity) value	39
Figure 26 3-D visualizations of resistivity patterns: Vertical exaggeration is 20	40
Figure 27 .Cross section of MRS hydrogeological layers and field plan location is depicted figure 2845	
Figure 28. Field plan and Location of cross sections A-A' and B-B'	46

Figure 29.3-D MRS Lithological model of the study area. Vertical exaggeration is 20..... 47
Figure 30. 3-D hydrogeophysical conceptual model..... 51

LIST OF TABLES

Table 1. Yellow River Basin water withdrawal, 1998-2000 (billion cubic meters)	6
Table 2. Applied geophysical methods and measured geophysical properties (from Drouart and Vouillamoz 2005).....	7
Table 3. The resistivity of some common rocks and minerals (from Baharuddin et al. 2018)	9
Table 4. Empirical NMR (MRS) relationship relating decay time rate with aquifer media (from Lubczynski and Roy 2003).	15
Table 5. Value of calibration coefficient CT assigned in different site	19
Table 6 Data Source and Format	25
Table 7 ERT Line information before and after editing.....	26
Table 8. Summary of the MRS investigations. Field camp: Field Campaign. S/N: Signal-to-noise ratio. EN/IN: External noise to instrumental noise ratio.....	29
Table 9. Rockworks Lithology type table	32
Table 10. The input data of 3-D lithology, 3-Resistivity Model and 3-D hydrogeophysical model.....	33
Table 11. ERT surveys with root mean square below than 8% after inversion	34
Table 12. MRS hydrogeological layer for plots with similar patterns versus depth. Spatial distribution of MRS field measurement can be found in Figure 28.....	43
Table 13. MRS hydrogeological layer for plots with inconsistent Patterns versus depth. Spatial distribution of MRS field measurement can be found in Figure 28.....	44
Table 14. Parameterization of MRS saturated layer (Layer2) using constant calibration coefficient (C_T): (a) longitudinal decay time constant (T_1) and (b) Using transverse decay time (T_2^*); S_y - Specific yield, θ_{MRS} -MRS free water Content; T_{MRS}, K_{MRS} -MRS estimates of Transmissivity and Hydraulic conductivity.	49
Table 15. Hydrogeophysical parameters for Maqu sub-catchment.....	50

1. Introduction

1.1. Background to subsurface hydrogeological modeling

Advances in groundwater modeling have been driven by the need to predict the impact of human activities and climate change on groundwater and associated environmental problems (Zhou and Li 2011). To develop an optimal groundwater management strategy, essential subsurface information is needed about geology and the hydrological conditions of the study area. Subsurface hydrogeological information are usually derived from different hydrogeophysical survey methods. A classic way of gathering subsurface hydrogeological data is through borehole drilling and associated aquifer test. However, this method is prone to high cost and time consuming to provide spatially distributed information because this method is commonly limited to the vicinity of the borehole. Non-invasive hydrogeophysical methods provide an efficient and economical way to get insights into subsurface hydrogeological conditions where boreholes data are not available (Baroncini-Turricchia et al. 2014). Hydrogeophysical methods provide a large-scale characterization of the subsurface hydrogeological properties under undisturbed conditions.

In the area where hydrogeological data are scarce like Maqu sub-catchment, hydrogeophysical methods are particularly suitable to characterize subsurface hydrogeological conditions that control behaviors of groundwater dynamics. The level of subsurface characterization required for a particular problem depends on many factors; the level of subsurface heterogeneity relatively to the characterization objective, spatial and temporal scales of interest (Hubbard and Linde 2011). Hence, in this work, two hydrogeophysical methods (Nuclear Magnetic Resonance Sounding and Electrical Resistivity Tomography) were used to characterize subsurface hydrogeological conditions of Maqu catchment. These methods were chosen according to their convenience to map subsurface hydrogeological setting and associated hydraulic parameters.

Representation of subsurface hydrogeology is often limited to 1D or 2D due to the lack of spatially distributed data even at the small catchment scale. Therefore, this study adopted the integral application of hydrogeophysical parameters and a geostatistical tool to predict spatial variability of hydrogeological layers. The subsurface hydrogeological presentation is usually performed using a combination of diagrams, cross sections and tables representing discretization of hydrogeological units (Lekula et al. 2017). A combination of GIS tools, 3D modeling software and elaboration of appropriate database helped to develop a comprehensive hydrogeological layering of the study area using hydrogeophysical dataset.

1.2. Problem description

In response to climate changes on Tibetan Plateau, elements of hydrological cycle have been affected such as, inhomogeneous distribution of precipitation or a slight increase of evapotranspiration due to a wetter ground surface inducing uncertainties for river discharge trends over the basins. Also, due to climate warming, maximum depth of snow has decreased, and thickness of active layer has increased in frozen ground, which imply changes in the water infiltrating the soil or forming direct runoff (Zhang and Guo 2011). Maqu sub-catchment is located on the eastern edge of Tibetan plateau in the upper part of Yellow River Basin, and it is considered as a source of Yellow River. Liu and Zheng (2004); Cuo et al. (2014) have reported that baseflow, groundwater flow, streamflow and surface runoff exhibit a strong decreasing trend over the main course of Yellow River in runoff production, mainly across the Maqu-Jimai section.

Although some hydrological studies present in the study area, most of them have been focused on streamflow climatology and its relation to precipitation and temperature changes (Cuo et al. 2014). There are only little studies to characterize subsurface hydrogeological conditions, which can provide valuable information on groundwater occurrence and enhance our understanding of groundwater flow dynamics at the catchment scale. Therefore, this study aims to understand the impact of subsurface hydrogeological conditions on groundwater occurrence, and later it can be used as a basis for detailed analysis on surface-groundwater interactions.

1.3. Assumption

Hydrogeophysical methods provide information related to a specific site during the instance at which measurement is being conducted. As the study area is characterized by seasonal variability of frozen and unfrozen soil conditions. The applied hydrogeophysical methods reflect only soil properties under unfrozen conditions because field measurements were conducted during the unfrozen period.

1.4. Research objectives

The overall objective of this study is to design a hydrogeophysical conceptual model by integrating various information from analyzing hydrogeophysical parameters.

Specific objectives related to Maqu sub-catchment are:

- i. To use hydrogeophysical methods of data acquisition to derive hydrogeophysical parameters;
- ii. To estimate subsurface hydraulic parameters using hydrogeophysical parameters;
- iii. To use hydrogeophysical parameters to characterize subsurface hydrogeological structure;
- iv. To apply geostatistical tool to predict spatial variability of hydrogeophysical layers.

1.5. Research questions

The overall research question is to explore how to establish a subsurface hydrogeological model in the Maqu sub-catchment?

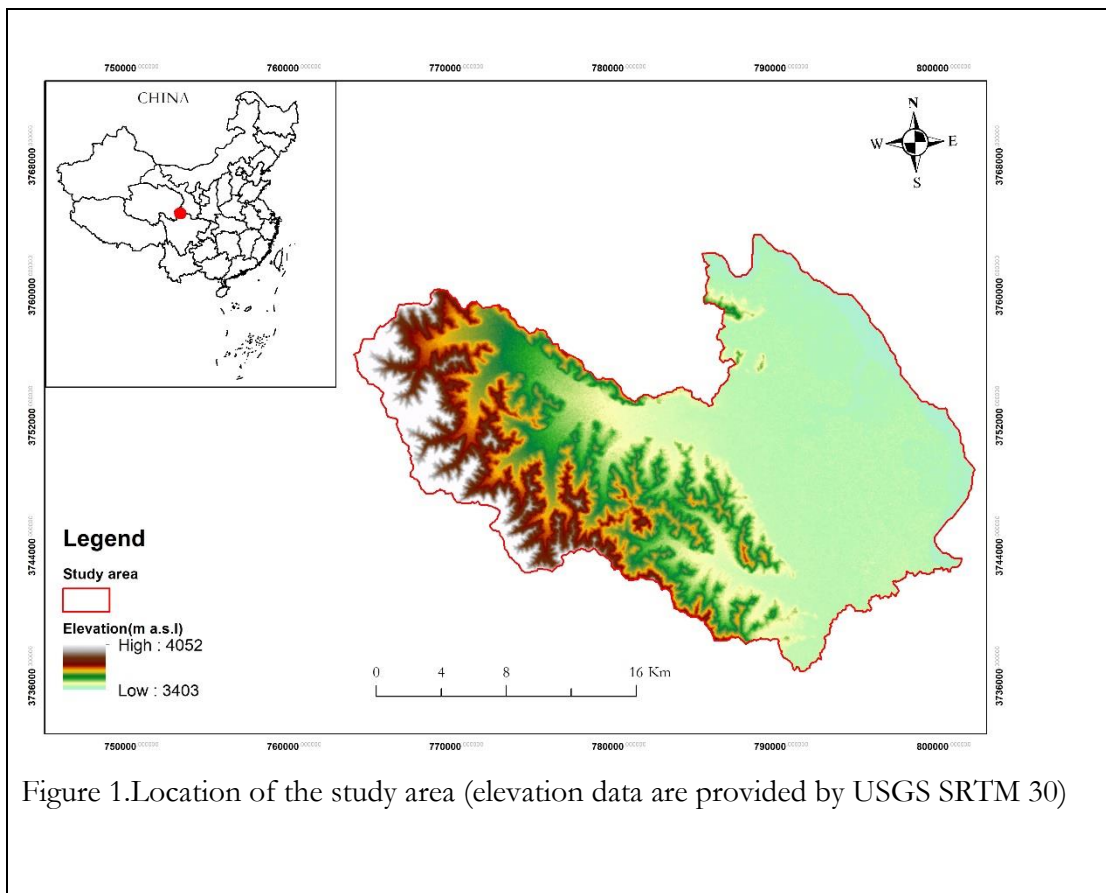
The specific questions addressed in this work are the following :

- i. How do integrated hydrogeophysical methods supplement each other to get insights into the subsurface hydrogeological setting?
- ii. What is the variation of hydrogeophysical parameters?
- iii. What is the most suitable algorithm to interpolate spatially distributed hydrogeophysical profiles?.
- iv. What is the spatial extent of hydrogeophysical layers?

1.6. Characteristics of the study area

1.6.1. Location

The study area is located in the upper river region of Yellow River Basin on the eastern edge of Tibetan Plateau , and the southwest of Gansu province in China and is extended within the following geographic coordinates $33^{\circ}06'30''$ - $34^{\circ}30'15''$ N, $100^{\circ}45'45''$ - $102^{\circ}29'00''$ E. The average elevation is approximately 3700m Mean Sea Level (M.S.L) as depicted in Figure 1.



1.6.2. Climate

The climate is cold and humid with an average annual temperature of 1.1°C and average annual precipitation of 615mm (Guo et al. 2012). The coldest month is January with an average temperature of -9.5°C, while the hottest month is July with an average temperature of 11.3°C. Precipitation mainly happens from May to September, accounting for about 82.7% of the whole year. Snow can occur in every month.

1.6.3. Hydrology

The study area is the upper part of the Yellow River Basin, and this River is the second largest river in China, and it is flowing through Maqu region with an approximate distance of 433 km. Maqu catchment is an important runoff collecting, water conserving and supplying area in the upriver region of the Yellow River Basin and it is considered as source Yellow River (Guo et al. 2012).

1.6.4. Geological setting

Geology of the study area is classified into three main categories such as ;(i) Before Quaternary system, (ii) Quaternary system, and (iii) Intrusive rock or granodiorite and each group can be further classified into subcategories and description of geology as follows:

(i) Before Quaternary system

- Permian System: the outcropped lithology is feldspathic quartz sandstone, sandy slate, and limestone; thickness is greater than 2392m.
- Triassic system: the outcropped lithology is limestone, feldspathic quartz sandstone, and sandy slate
- Jurassic system: the outcropped lithology is conglomerate and sandstone; thickness is greater than 488m.
- Cretaceous system: the outcropped lithology is conglomerate and sandstone; thickness is greater than 1677m.
- Neogene System: the outcropped lithology is sandstone, conglomerate, and mudstone; thickness is greater than 193m.

(ii) Quaternary system

- Upper Pleistocene: conglomeratic silt with sand, gravel, and boulder; thickness is about 50—60m.
- Holocene series: sand and detritus; thickness is about 5—20m.

(iii) Intrusive rock

- Clastic rocks: including rocks from Neogene System, Cretaceous system, and Jurassic system.
- Carbonate rocks: including rocks from Permian System and Triassic system.
- Magmatic rock: granodiorite.

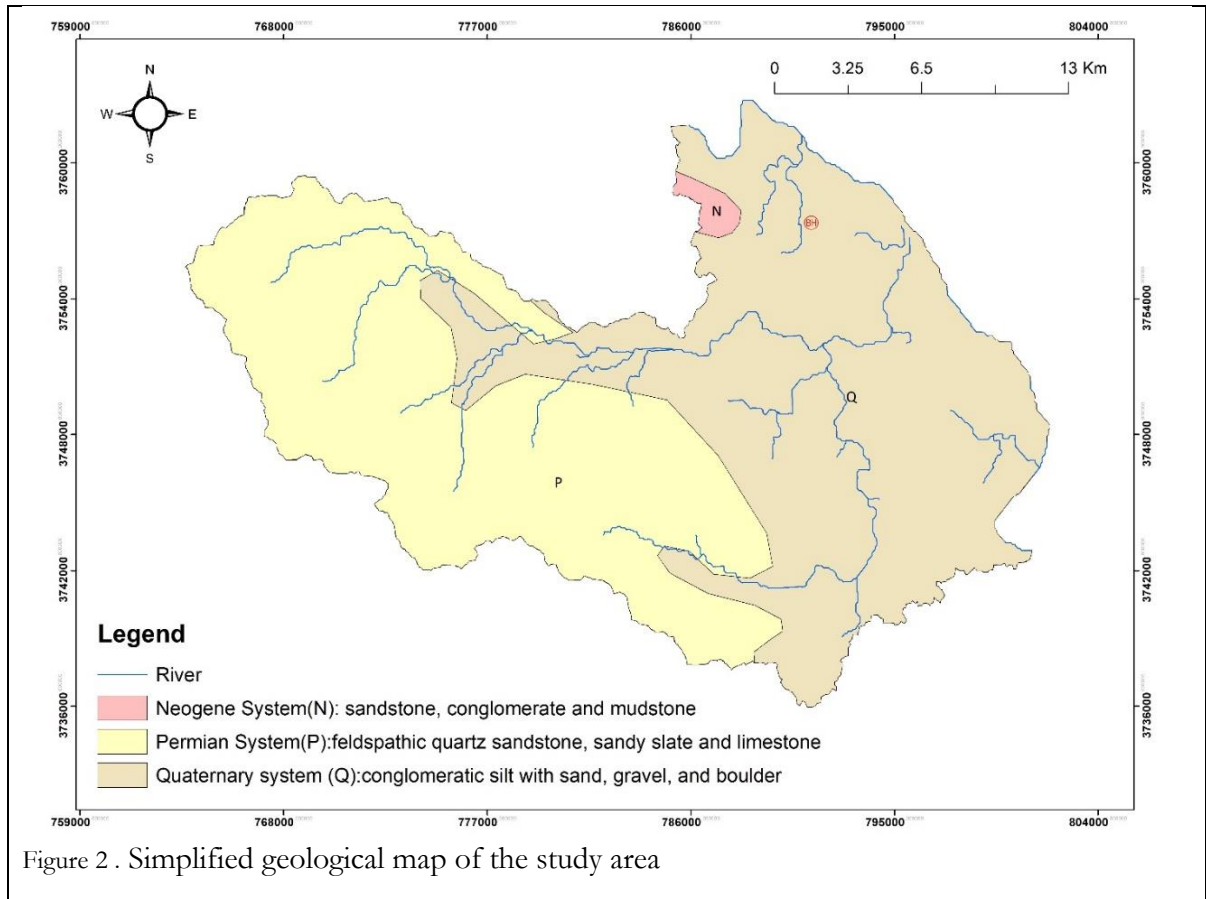


Figure 2 . Simplified geological map of the study area

2. Previous hydrological studies in the study area

The study area is characterized by limited studies on hydrogeological processes as most researchers have been focused on streamflow climatology and its relation to precipitation and temperature changes (Cuo et al. 2014). Groundwater studies were roughly estimated over the river basin scale. For instance, Zhang and Guo (2011) studied the variability of water resources in the Yellow River Basin over the past fifty years and reported that streamflow exhibit decreasing trends and water resource deficit tend to be more sensitive from upstream to downstream with some zero-flow measurement during 1990-2000 mainly in spring and summer periods. Those low flow events were associated with climate changes and the impact of human activities compared to high flow events.

According to Cuo et al. (2014), the reduction in streamflow is due to dual effects of increasing evapotranspiration and decreasing of precipitation in the main river runoff production section of Maqu-Jimai particularly between July and September and increasing of anthropogenic activities in the lower part of the basin. UNESCO (2010) pointed out that the annual runoff reduction in the lower part of Yellow River Basin is approximately 5.6 billion m^3 and this is due to the impacts of climate changes and land-use cover change.

Giordano et al. (2004) reported that water use in the Yellow River Basin could be divided into two sources such as ground and surface water to supply three main sectors: agriculture, industry and domestic. The average annual river withdrawal from river basin has been approximately 50 Billion Cubic Meter (bcm) with 74 percent and 26 percent from surface and groundwater respectively, where agriculture is the largest withdrawal accounting 80 percent of total consumption as shown in Table 1.

Table 1. Yellow River Basin water withdrawal, 1998-2000 (billion cubic meters)

Year	By Source			By Sector				
	Surface water	Groundwater	Total	Ag.	Ind.	Urban	Rural	Total
1998	37	12.7	49.7	40.5	6.1	1.6	1.5	49.7
1999	38.4	13.3	51.7	42.6	5.7	1.8	1.5	51.7
2000	34.6	13.5	48.1	38.1	6.3	2.1	1.6	48.1
Average	36.7	13.2	49.8	40.4	6	1.8	1.5	49.8
Share	74%	26%	100%	81%	12%	4%	3%	100%

(from Giordano et al. 2004)

3. Hydrogeological characterization with geophysical methods

Hydrogeophysical methods provide physical characteristics of the subsurface structure such as resistance, the speed of propagation of sound, density, magnetism and conductivity (Baharuddin et al. 2018). Those physical properties are influenced by porosity, the volume, and quality of water it contains (Drouart and Vouillamoz 2005). Each hydrogeophysical method has its characteristics and owns capabilities to characterize subsurface hydrogeology. Thus, the choice of appropriate method depends on the modeling objective and geological setting of the study area (Francés et al. 2014).

In comparison to other methods, Magnetic Resonance Sounding (MRS) can be classified as a direct hydrogeophysical method because it measures signals emitted by the water molecule's hydrogen nuclei (Lubczynski and Roy 2005). The contribution of MRS to hydrogeology is the ability to measure a signal indicating the existence of groundwater (Drouart and Vouillamoz 2005). However, some geological constituents have similar or overlapping geophysical properties. Therefore, it is advisable to use more than one method to acquire a unique signature of the different geological unit (Chirindja et al. 2016). Two Dimensional Electrical Resistivity Tomography (2D ERT) technique have been routinely used in groundwater studies to provide supporting information to constrain aquifer geometry, storage, and flow properties. ERT is capable of detecting water-saturated clay through the variations of resistivity with depth at the surveying profile (Hazreek et al. 2018). However, the resistivity of water-bearing rock does not only depend on the amount of water it contains. The chemical composition and temperature can

affect distribution patterns of subsurface resistivity. 2D ERT can be considered as a geophysical reference method because it can be used in a wide range of contexts (Drouart and Vouillamoz 2005).

In general hydrogeophysical characterization can be categorized into the following main objectives (Hubbard and Linde 2011).;

- ❖ Hydrological mapping of subsurface features (Interface between geological unit, water table);
- ❖ Estimating subsurface properties or state variable (Water content) that influence groundwater flow and storage.
- ❖ To monitor subsurface hydrological process (like infiltration through the vadose zone and tracer migration).

Table 2. Applied geophysical methods and measured geophysical properties (from Drouart and Vouillamoz 2005).

Method	Measured geophysical parameter	Operational physical properties	Influence of groundwater
ERT	Potential difference due to electric currents	Electrical Resistivity	Indirect
MRS	Proton magnetic relaxation signal in water	Spin and Magnetic moment of the hydrogen nucleus	Direct

3.1. Electrical Resistivity Tomography (ERT)

3.1.1. Introduction to resistivity measurement

Resistivity measurements are made by feeding current into the ground through one pair of electrodes (current electrodes) while the resulting voltage is recorded by another pair of electrodes (Potential electrodes). Because the current is measured as well, an apparent resistivity of the subsurface can be estimated, and the nature and structure of aquifers are then deduced based on the subsurface resistivity contrast (Loke 2004). By referring to (Loke 2004) the apparent resistivity of the soil formation through which the current passes is calculated using Equation 1.

$$\varphi = K \frac{\Delta V}{I} \quad \text{Equation 1}$$

Where φ is the value of apparent resistivity in ohm-meters (Ohm.m), I is electrical current in amperes (A), ΔV is the potential difference in volts (V), and K is the geometric factor which is depends on the geometrical configuration of electrodes. The resistivity (φ) is called “apparent resistivity” because it represents the resistivity of the whole set of the subsurface formation through which the current flows, which can be different from the real resistivities of each formation layer (Drouart and Vouillamoz 2005). In this case, the actual volume of each soil formation involved in measurement is known and the penetration depth is proportional to the spacing between electrodes (Dahlin 2001).

Different terms are used to describe different type of resistivity data acquisition such as (1) 1D survey method which is carried out either by profiling or Vertical Electrical Sounding (VES). Profiling method is carried out by moving electrode at constant spacing along a straight line and plotting the variation of resistivity against profiled distance. This gives information about lateral changes of resistivity, but it cannot characterize vertical variation. Nevertheless, VES can be also used to characterize vertical stratification, via increasing the electrodes separation distance around a mid-point. The major limitation with VES method is that it does not take into account lateral inhomogeneity in subsurface layering, which is most commonly found in nature. (2) 2-D ERT method has been developed to take into account both lateral and vertical variation of resistivity in soil formation, but it does not consider lateral changes in a direction perpendicular to the survey line. This method requires the data to be recorded by multiple electrodes lying along a line to be surveyed with an automatic selection of pairs of currents and potential electrodes to supply the current and records electrical potential difference respectively. (3) 3D survey (electrical resistivity tomography or imaging) method is built up based on a grid of electrodes, and measurement is taken with electrodes aligned in different directions (Loke 2004), but the practical application of this method is still limited due to the high demand for computational power and associated cost (Dahlin 2001).

Therefore, the 2-D survey method is the preferable method regarding very accurate results and maintaining affordable survey cost. But the practical application of this method has some constraints such as; the influence of electrical cable located beneath and above the ground surface, topographical undulation, and vegetation disruption. Thus, it is essential to select a potentially favorable site rather covering large scale (Drouart and Vouillamoz 2005). Technical constraint associated with resistivity survey is that it offers a limited resolution with depth due to the decreasing sensitivity with increasing of distance away from the electrodes. The main practical applications of electrical resistivity in hydrogeology are :

- Delineation of the lithological unit,
- Investigation of depth and thickness of aquifers and aquicludes as well as the weathering layer above the bedrock
- Mapping of saltwater intrusions
- Detection of fracture and faults zones
- Mapping of preferential water pathways
- Detection of cavities

By calculating true subsurface resistivity distribution, it gives the possibility of locating groundwater by taking into considerations the following subsurface properties (Prachi and Adamane 2015):

- A hard rock without pores or fractures and dry sand without water or clay are very resistive;
- A porous or fracture rock bearing free water has a resistivity which depends on the resistivity of water and the porosity of the rock;
- An impermeable clay layer, containing bound water, has a low resistivity;
- Mineral ore bodies (Iron, Sulphide, etc.) have very low resistivity due to their electric conduction property.

The following factors can contribute to the reduction of electrical resistivity of soil's formation (Wiese 2012):

- Additional pore-fluid;
- High salinity fluid;
- Increased fracturing (Weathering) and interconnection between pores;
- Additional clay content;
- Increased temperature.

And resistivity of earth materials increases with the greater level of compaction and lithification (Where pores are blocked by mineral deposition).

Table 3. The resistivity of some common rocks and minerals (from Baharuddin et al. 2018)

Rocky Type	Resistivity (Ohm.m)
Igneous/Metamorphic	
Granite	$5 \times 10^3 - 10^8$
Weathered granite	$1 - 10^2$
Basalt	$10^3 - 10^6$
Quartz	$10^3 - 2 \times 10^6$
Marble	$10 - 2.5 \times 10^8$
Schist	$20 - 10^4$
Sediments	
Sandstone	$8 - 4 \times 10^3$
Conglomerate	$2 \times 10^3 - 10^4$
Shale	$20 - 2 \times 10^3$
Limestone	$50 - 4 \times 10^2$
Unconsolidated sediment	
Clay	$1 - 100$
Alluvium	$10 - 800$
Clay (Wet)	20
Groundwater	$10 - 100$
Marl	$1 - 70$
Fresh water	$10 - 100$

3.1.2. Resistivity measurement procedure with 2D Survey

2D Electrical Resistivity Tomography (ERT) is carried out using multiple electrodes of four-electrodes measurement (Ling et al. 2016). 2D resistivity survey is conducted using multiple electrodes connected to a multi-core cable, a laptop computer connected to an electronic switching unit which is used to select the appropriate four electrodes automatically for each measurement. However, some field systems have an in-built microprocessor system, so that a laptop computer is not needed. The spacing between electrodes can be less than one meter up to hundreds of meters. Figure 3 shows an example of an electrode

configuration for 2-D resistivity survey with electrodes along a straight line and a multi-electronic cable connected to the electronic switching unit together with a computer laptop.

Figure 3 adapted from Loke (2004) shows a schematic arrangement of electrodes for field measurement. The first measurement is made by four electrodes where electrode 1 serves as the first current electrode and electrode 2 and three as first and second potential electrodes respectively, and electrode 4 is the second current electrode. For the second measurement, electrode 2,3,4, and five are used with same procedures as the first measurement; this is repeated throughout the survey line until the last 4 electrodes are used for the last recording with “1a” spacing. After completion of sequence measurement with “1a” spacing, the next measurements are conducted using a spacing of “2a” between electrodes. Therefore, the first measurement for 2a spacing uses electrodes 1,3,5, and 7 and the electrodes must be chosen so that the spacing between two adjacent electrodes is “2a”. For the second measurement electrodes 2, 4, 6 and eight are used. The process is repeated throughout the survey line until the last measurement is taken with “2a” electrode spacing. The same process is repeated for another measurement by considering other possible spacing between electrodes (“3a”, “4a”, “5a” and “6a”). The number of measurement obtained for each electrode spacing depends on the type of configuration used.

Different type of electrodes configurations are frequently used in practice; (1) Wenner, (2) dipole-dipole (3) Wenner-Schlumberger (4) pole-pole and (5) pole-dipole (Loke 2004). The choice of appropriate configuration for field survey depends upon onsite conditions, information needed and the sensitivity of the resistivity meter (Baxter et al. 2008).

Other characteristics to be considered for selecting array configuration for field data acquisition are (1)the depth of investigation, (2) the sensitivity of electrode configuration to both horizontal and vertical changes (3) horizontal data coverage and (4) the signal strength. In practice, Wenner configuration is a suitable choice, if the vertical resolution is required whereas Dipole-dipole configuration might be a good choice if a good horizontal resolution and data coverage are required. The 2D survey is a suitable method to provide supporting information to other hydrogeophysical methods for subsurface hydrogeological interpretation and parameterization (Loke 2004).

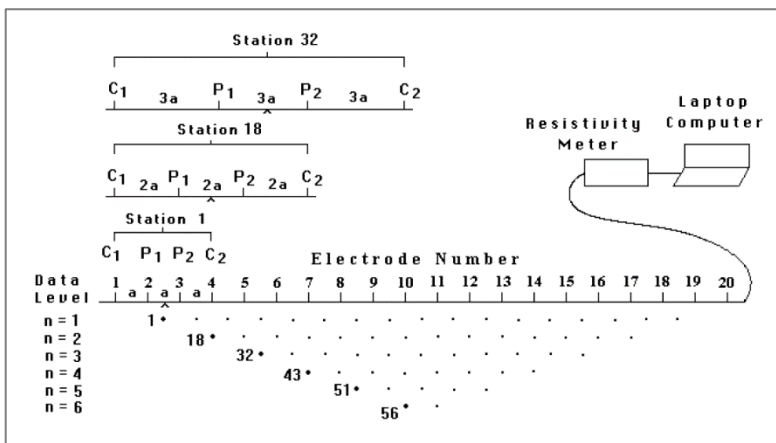


Figure 3. The arrangement of electrodes for a 2 D ERT survey and the sequence of measurement used to build up a pseudo section (from Loke 2004).

3.1.3. Data processing and presentation

Once the data set is collected, a reconstruction process is required which turns the field measurement (apparent resistivity) into the 2D image of subsurface resistivity distribution. This process involves two main simultaneous steps; forward modeling and inverse modeling. Forward modeling consists of deriving a theoretical response from a set of inputs parameters (electrode configuration, field measurement, and other boundary conditions) into the modeling software by applying a mathematical model. This involves solving the differential equation (Poisson equation; Equation 2) which governs the flow of electrical current in the ground.

$$\nabla^2 \varepsilon V = I \delta(\vec{r} - \vec{r}_s) \quad \vec{r}, \vec{r}_s \in \Omega \quad \text{Equation 2}$$

Where ε is the conductivity (which varies as a function of position), V is electric potential, $\vec{r}_s = (x_s, y_s, z_s)$ is the location of the current electrode in Ω . This equation can be solved analytically or approximately using numerical approaches. In practice, numerical approach is most frequently used (Wiese 2012). Numerical solution for forward modeling comprises multiple methods including; finite difference and finite element methods (Silvester and Ferrari 1996). With advances in computer processing, those equations are solved using computer based tools which give a more realistic subsurface resistivity distribution with minimum inputs from the user.

Inverse modeling is the practice of reconstructing theoretical resistivity distribution derived from measured values to build 2D resistivity image. In theory, inversion allows predicting a particular spatial distribution of physical properties. This is a problematic task because of: i) Different errors associated with the field measurement, ii) Non-uniqueness of model response, iii) There is often more free model parameters than independent data points. Inversion theory deals with these problems by implementation of inversion regularization schemes (Constraints, damping, smoothing). This is a complex process because if too much regularization is applied the model doesn't reflect true subsurface resistivity distribution whereas if too little is applied the inversion may become unstable and do not converge to a minimum in the data misfit (Wiese 2012). Therefore, During the inversion process, we seek to find a model that best first between measured and modeled value usually in the least square sense (Loke 2013).

The apparent resistivity is represented as point measurement on pseudosection or pseudo depth graph which depict the location of the measured value in 2D dimensions. Pseudosection or 2D profile are used to visualize the location of the measured value. The most useful practical application of pseudosection is that it helps to pick out bad points which are characterized by unexpected measurement with high or low values (Loke 2004) and those bad points are associated with two types of errors which can occur during field data acquisition such as; Systematic or Random error (Loke 2013). After interpretation, the calibration process is required because geophysical measurement has hydrogeological meaning after calibration with other geological knowledge about the specific site (Drouart and Vouillamoz 2005).

3.2. Magnetic Resonance Sounding (MRS)

3.2.1. Background and field measurement procedures

One dimensional application of Surface Nuclear Magnetic Resonance (NMR) is commonly called Magnetic Resonance Sounding (Costabel and Günther 2014). This method uses a large loop of wire laid on the ground surface to activate and detect the existence of water molecule's hydrogen nuclei at the resonant frequency which is proportional to the earth's magnetic field (Walsh et al. 2014). Thus, this method has the direct ability to detect subsurface water presence through the excitation of hydrogen protons (Bernard et al. 2006). The loop on the ground surface is energized by a pulse of an alternating current oscillating at the resonant frequency as follows;

$$i(t) = I_0 \cos(\omega_0 t) \quad \text{Equation 3}$$

Where I_0 is current amplitude and ω_0 is the frequency that generates an alternating magnetic field in the subsurface (Legchenko et al. 2010) and this magnetic field modifies the state condition of hydrogen protons. In addition, it is known that under equilibrium conditions, the hydrogen protons have a magnetic moment that is aligned with local earth's magnetic field. Upon excitation, the axis of the precession is modified. Thus, to carry out field measurement it is necessary to know the magnitude of local earth's magnetic field (B_0). When applied field is abruptly turned off the hydrogen protons return to their equilibrium position with a relaxation signal characterized by an initial amplitude and decay time as follows (Roy and Lubczynski 2014);

$$e(t) = E_0 \exp(-t/T_d^*) \cos(2\pi f_L t + \varphi_0) \quad \text{Equation 4}$$

Where E_0 is initial amplitude, t is the time, T_d^* is free induction decay time constant or relaxation time constant, f_L is larmor frequency and φ_0 is a phase shift between signal and excitation pulse (Lubczynski and Roy 2004). Through this processes of absorption and relaxation, the NMR measurement causes the water itself to produce a weak but detectable alternating magnetic field which is recorded by the same loop (Walsh et al. 2014). One sounding is composed by signals measured with different value of pulse moment (q).

$$q = I_0 \tau \quad \text{Equation 5}$$

Where I_0 is current amplitude and τ is the duration of the pulse of alternating current.

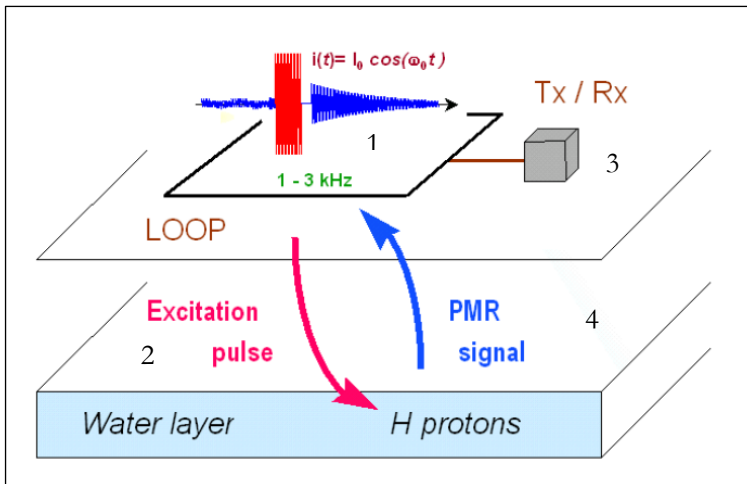


Figure 4. General principle and configuration of MRS : 1: Antenna, 2: promotion of energy generated by the device Tx (3), 4: MRS signal generated by hydrogen protons and taken by the device (from Bernard et al. 2006).

The depth of investigation depends on MRS loop size and shape; the magnitude of pulse moment; and electrical conductivity of subsurface formation (Lubczynski and Roy 2007).

Before the execution of MRS, the following practical advice should be conducted (MICHELS 1997):

- Verification of magnitude of the local earth magnetic field which is necessary to calculate Larmor frequency. Therefore, the Larmor precession frequency (f_L) is directly proportional to the site-specific earth's magnetic field (B_0) and is determined by the following relation:

$$f_L = \omega_0 / 2\pi = \gamma B_0 / 2\pi \quad \text{Equation 6}$$

Where γ is the gyromagnetic ratio for hydrogen protons ($\gamma = 0.267518 \text{ Hz/nT}$) (Pehme 2011). Additionally, the Larmor frequency depends on earth's magnetic field, this implies its variation with a location between 1kHz to 3 kHz where the earth's magnetic field is weak towards the equator and is too high towards the poles (Walsh et al. 2014)

- Verification of electromagnetic noise before starting MRS measurement. It allows to estimate the signal-to-noise ratio (S/N); as a ratio of the amplitude of the magnetic resonance signal to a mean of the electromagnetic noise.
- Measurement of magnetic susceptibility of the subsoil because the presence of magnetic rocks may modify earth's magnetic field and it is assumed that during field measurement earth's magnetic field is constant (Legchenko et al. 2010).

3.2.2. Data inversion

After field data acquisition, inversion of the records is usually performed using one-dimensional inversion software included in the equipment package. During the inversion of MRS records (signal amplitude and relaxation time), three main parameters are derived (Lubczynski and Roy 2004);

- The MRS free water content (θ_{MRS}) which is closely related to the MRS initial signal amplitude (E_0) and is represented as a percentage of water content versus depth and it is defined as the volume of water with sufficient long decay time over the total volume sampled by the sounding (Vouillamoz et al. 2008).
- The MRS free induction decay time constants or relaxation time constants (T_2^* and T_1) which are related to the mean size of pores that contain the water molecule's hydrogen nuclei (Lubczynski and Roy 2005). With T_2^* which is the transverse decay time constant and it is related to the component of proton magnetic moment that is perpendicular to the earth's magnetic field whereas T_1 is longitudinal decay time constant which is related to the component of proton magnetic moment that is parallel to earth's magnetic field (Bernard et al. 2006).
- The phase shift (φ_0) between the relaxation signal and the excitation current which is linked to ground electrical conductivity (i.e., resistivity).

And the following main graphs are usually used to illustrate the distribution of MRS outputs as a function of depth:

- The sounding curve, which depicts the initial amplitude of the relaxation signal as a function of pulse moment and this gives an initial qualitative picture of amount water content as a function of depth
- Geophysical interpretation curves, which depict the free water-content and decay time constants as a function of depth.

To convert MRS derived parameters (free water content and relaxation time constant) into hydrogeological properties, calibration process at the same site is usually performed because no universal quantitative formulation has been proposed yet.

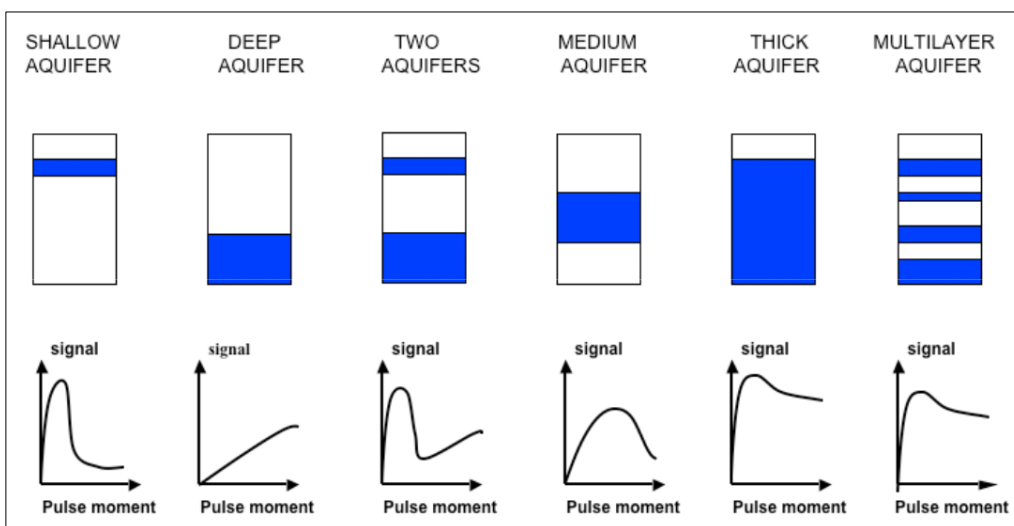


Figure 5. MRS signal amplitude curve for different aquifers, various types of thickness and depths (from Bernard et al. 2006).

3.2.3. Hydrogeological parameterization with MRS

MRS provides insight into subsurface hydrogeophysical parameters as a function of depth. This information can be used to determine the hydrogeological setting of the aquifer at the specific site due to strong physics foundation linking MRS outputs and both groundwater storage and flow properties (total and effective porosity, specific yield, and hydraulic conductivity: Lachassagne et al. 2005; Lubczynski and Roy 2005, 2007).

Initially, MRS was used to characterize hydrogeological parameters of the saturated zone, but recent research has proven that it can be used to provide useful information for hydrogeological parameterization of unsaturated or vadose zone (Walsh et al. 2014). Hydrogeophysical parameters derived from MRS signals are; MRS free water content (θ_{MRS}), the longitudinal decay time constant (T_1), and transverse decay time constant (T_2^*) versus depth. Measurement of T_2^* is easier and faster than T_1 because measuring T_1 requires the application of two pulses moment with a variable delaying between them. But, T_2^* is also affected by local inhomogeneity of the earth's magnetic field. However, in area where the subsurface composition is characterized by materials with low magnetic susceptibility T_2^* can be reliable for hydrogeological parameterization (Mazzilli et al. 2016).

Decay time constants are affected by the mean distance between the water molecules and the surface of the solid particles. Therefore, decay time can be correlated to pores size distribution and degree of saturation because in unsaturated zone water remains to solid particles surface due to capillary forces: the shorter the distance, the shorter the relaxation time constants (Mazzilli et al. 2016). Thus, the relaxation time is an indication of how groundwater is extractable (Lubczynski and Roy 2004). Table 4 shows the empirical relationship between decay time constant (T_2^*) and the lithology of the aquifer media.

Table 4. Empirical NMR (MRS) relationship relating decay time rate with aquifer media (from Lubczynski and Roy 2003).

Signal decay rate	Petrophysical information	MRS detectability
$T_2 < 3\text{ms}$	Clay bound water	No
$T_2^* < 30\text{ms}$	Sandy clays	No or Marginally
$30 < T_2^* < 60\text{ms}$	Clayey sands, very fine sands	Yes
$60 < T_2^* < 120\text{ms}$	Fine sands	Yes
$120 < T_2^* < 180\text{ms}$	Medium sands	Yes
$180 < T_2^* < 300\text{ms}$	Coarse and gravely sands	Yes
$300 < T_2^* < 600\text{ms}$	Gravel deposits	Yes
$600 < T_2^* < 1500\text{ms}$	Surface water bodies	Yes

The measured MRS free water content (Θ_{MRS}) is defined as the volume of water with long decay time (sufficiently to be measured by the instrument) over the total sampled volume (Vouillamoz et al. 2012) and is assumed to be equal to the subsurface free water content (Φ_f) mainly for sandstones and quartz-rich clastic due to the instrument dead-time which is in order of 30ms to 40ms and prevent the detection of faster decaying MRS signal in small pores. However, recent research by Walsh et al. (2014) has proven that MRS signal with faster decaying time can also be detected within an unsaturated zone with an instrument's dead-time below 10ms. The dead time is defined as the time it takes for the instrument to switch between transmitting and receiving of MRS signals. Subsurface free water content (Φ_f) represents the amount of water content that can move within the rock either by gravity or pressure gradients (Lubczynski and Roy 2007). In saturated zone subsurface free water content consists of effective porosity (n_e), unconnected and dead end pores (Lubczynski and Roy 2003).

Specific yield (s_y) is an important parameter for groundwater storage which indicate the amount of water that can be released by gravity when an unconfined aquifer is drained and the remaining quantity after it is fully desaturated is expressed as specific retention (s_r) also know as field capacity . The two terms effective porosity (n_e) and specific yield (s_y) are commonly confused but effective porosity is the ratio of speeds whereas specific yield is the ratio of volume; effective porosity (n_e) is defined as the ratio between the volume of mobile water in a saturated zone to the total volume of the rock under investigation. while pecific yield (s_y) is defined as the volume of water a rock releases by gravity forces to the total volume of drained rock in an unconfined aquifer.

Total porosity (n) is expressed quantitatively as a ratio of the volume of voids to the total volume of the medium under investigation. Thus, effective porosity (n_e) is less than to total porosity(n). A complete discription of the concept of aquifer water storage have been explained by Lubczynski and Roy (2003) as depicted in Figure 6.

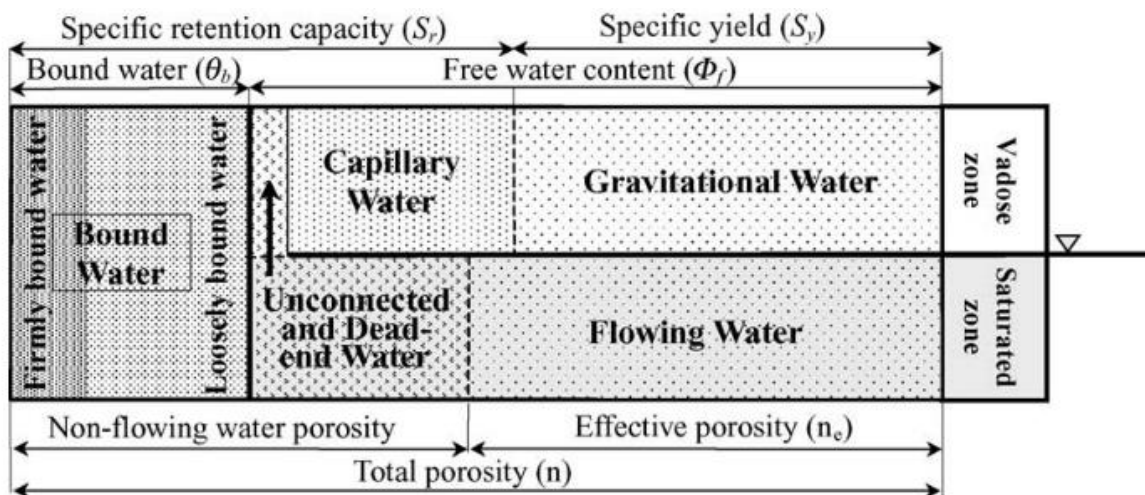


Figure 6. Aquifer groundwater storage concept (after Lubczynski and Roy 2003)

According to Vouillamoz et al. (2012) MRS free water content (Θ_{MRS}) is approximately equal or greater than to effective porosity (n_e) and specific yield (s_y) for coarse grained rocks ($\Theta_{MRS} \approx n_e \geq s_y$) but n_e differs from s_y in fine grained rocks. The same principle has been explained by Lubczynski and Roy (2005) if the MRS test is performed over a rocky medium where MRS free water content (Θ_{MRS}) is approximately equal to effective porosity (n_e). In the case of an unconfined aquifer composed by coarse and permeable rocks under the assumption of $\Theta_{MRS} \cong \phi_f$, the specific yield can be calculated using the following equation;

$$s_y = \Theta_{MRS} - s_r \quad \text{Equation 7}$$

Where s_r is consist of bound water and portion of free water content retained agaisnt gravity as shown in Figure 6. The same approach can be applied in case of a confined aquifer to estimate storage properties i.e: elastic storage and specific drainage (Lubczynski and Roy 2005). However, the practical determination of specific retention(s_r) prevent the direct use of Equation 7 to determine specific yield from MRS free water content. Vouillamoz et al.(2007) proposed an empirical approach for determining MRS storage parameters for unconfined and confined aquifer using Equation 8 and Equation 9 respectively:

$$s_{yMRS} = C_y \Theta_{MRS} \quad \text{Equation 8}$$

$$s_{eMRS} \cong C_e (\Theta_{MRS} \Delta Z_{MRS}) \quad \text{Equation 9}$$

Where s_{yMRS} is the MRS specific yield, s_{eMRS} is the MRS specific storage, ΔZ_{MRS} is the thickness of MRS saturated layer, C_y and C_e are parametric factors which are depend on the geological context. In literature the value of C_y and C_e are currently not available for various lithology except weathered granite materials of BurukinaFaso where the value of C_y can be found in Vouillamoz et al.(2007). Therefore, tho se empirical storage multipliers invalidate the application of those equations to any other site where validation parameters are not available.

Vouillamoz et al. (2012, 2014) also proposed a new approach of using decay time constant to evaluate MRS storage properties because decay time is influenced by the geometry of pores and the degree of saturation of the medium under investigation. This approach helps to discriminate the MRS signal generated by gravitational water in saturated zone from the signals generated by capillary water or bound water in the vadose zone using the principle of apparent cutoff time values (ACT) of decay time. But, the provided empirical relationships between specific yield and decay time also depend on the geological context, and further improvement is also required for the universal application.

Boucher et al. (2009) proposed an other approach of estimating specific yield based on the assumption that the amount of undetectable water by MRS ($\Theta_u = n - \Theta_{MRS}$) and specific retention follow a similar pattern as a function of grain size for aquifer composed mainly by fine sands in the southernwest of Niger. The hypothesis was created based on the fact that the amount of undetectable water is depends on the mean relaxation time(T_2^*), which itself controled by the pore size of the aquifer. Thus, a parametric

model of s_r and θ_u changes as a function grain size was established which resulted in a relationship between MRS water content and specific yield as shown in Figure 7.

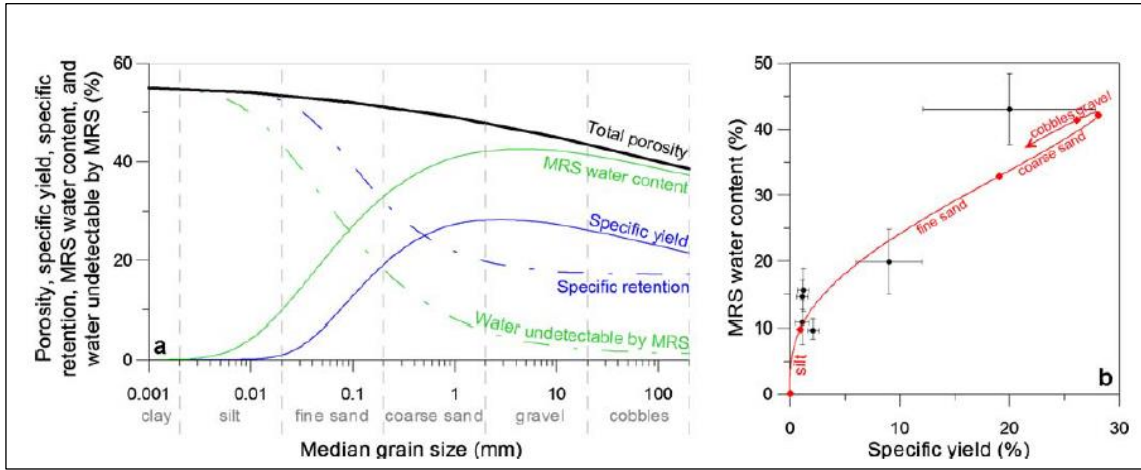


Figure 7. A model relating total porosity, specific yield, specific retention, MRS water content and undetectable water by MRS as a function of grain size and corresponding diagram of the MRS water content as function specific yield (Adapted from Boucher et al. 2009).

Besides aquifer storage parameters that can be calculated from MRS signals, also aquifer flow parameters have been successfully estimated from MRS signal for saturated rocks (e.g., Vouillamoz et al. 2014; Baroncini-Turricchia et al. 2014; Francés et al. 2014; Lubczynski and Roy 2005). The relaxation time is linked to the mean size of pores that contain water. Therefore, it can be used to estimate aquifer flow parameter. To retrieve flow parameters from the MRS signal, the following empirical equations are usually used:

$$T_{MRS} = C_T \theta_{MRS} T_d^2 \Delta Z_{MRS} \quad (\text{SeEVERS}) \quad \text{Equation 10}$$

$$T_{MRS} = C_T \theta_{MRS}^4 T_d^2 \Delta Z_{MRS} \quad (\text{KENYON}) \quad \text{Equation 11}$$

$$K_{MRS} = \frac{T_{MRS}}{\Delta Z_{MRS}} \quad \text{Equation 12}$$

Where T_{MRS} , K_{MRS} are the MRS hydraulic transmissivity (m^2/s) and conductivity (m/s) respectively, ΔZ_{MRS} , θ_{MRS} and T_d are the MRS saturated layer thickness; MRS free water content (%); and decay time constant (ms) respectively, and C_T (m/s^3) is a calibration coefficient which is calculated by comparing MRS transmissivity to the transmissivity obtained with pumping test at the same site. Therefore, it depends on the geological setting of the site under investigation and in literature, it is reported to vary between $\sim 10^{-10} \text{m}/\text{s}^3$ to $\sim 10^{-6} \text{m}/\text{s}^3$ depends on rock type (Boucher et al. 2009).

$$C_T = \frac{T_{Pt}}{\theta_{MRS} T_d^2 \Delta Z_{MRS}} \quad \text{Equation 13}$$

With T_{Pt} (m/s^2) which is the transmissivity from pumping test. The fact that the calculation of C_T requires an evaluation of MRS transmissivity from nearby pumping test, this prevent the direct use of this equation to any other site where pumping test data are not available. However, little information about the calibration coefficient for various lithology have been published and are presented in Table 5.

Table 5. Value of calibration coefficient C_T assigned in different site

$C_T(10^{-9})$ With T_2^*	$C_T(10^{-9})$ With T_1^*	Lithology
0.0028		Limestone, sand, clay (Legchenko et al. 2002)
	0.000153	Limestone, sand, clay (Legchenko et al. 2002)
0.062		Fractured granite (Legchenko et al. 2002)
0.568		Fractured diorite (Legchenko et al. 2002)
	0.9	Fine sands with clay (Plata and Rubio 2008)
1.3		Clay-sandy, weathered and fractured rocks (Vouillamoz et al. 2009)
2.99		Limestone, sand, clay (Legchenko et al. 2002)
	0.165	Limestone, sand, clay (Legchenko et al. 2002)
32.6		limestone, chalk (Legchenko et al. 2002)
	500	gravel with clay (Plata and Rubio 2008)

Table 5 shows the variation of C_T with lithology but it even depicts inconsistency of C_T value for similar lithology depends on decay time constant applied . Therefore, the value of C_T is mostly depends on geological context. Plata and Rubio (2008) proposed a different approach of using a parametric function for determining the calibration coefficient C_T with the following equation.

$$C_T(F) = mF^{-n} \quad \text{Equation 14}$$

Where $F = \theta_{MRS} T_d^2 \Delta Z_{MRS}$, and m and n are fixed values estimated by evaluating MRS parameters with associated pumping test at different sites but there is no clear guideline for calculating those coefficients, probably they are depend on geological context.

Equation 10 and Equation 11 can take different form depending on the type of decay time constant selected ($T_{MRS} = C_T \theta_{MRS} T_1^2 \Delta Z_{MRS}$; $T_{MRS} = C_T \theta_{MRS}^4 T_1^2 \Delta Z_{MRS}$; $T_{MRS} = C_T \theta_{MRS} T_2^{*2} \Delta Z_{MRS}$; $T_{MRS} = C_T \theta_{MRS}^4 T_2^{*2} \Delta Z_{MRS}$).

4. THREE-DIMENSIONAL HYDROGEOLOGICAL MODELLING

Significant advances in computer-assisted processing and development of 3D modeling software tools, as well as the recently increased 3D geographic information system application, has driven the use of 3D hydrogeological model as a tool for subsurface hydrogeological visualization (Raju et al. 2015). The computer has allowed to manipulate, store and analyze a huge amount of datasets that previously took a long period (Thorleifson et al. 2007). 3D modeling software and visualizations tools (RockWorks, GoCAD, EVS/MVS) using geostatistical algorithms are available and are widely used for hydrogeological modeling. However, a proper selection of a particular approach for the design of 3D model depends upon the site, data availability, and complexity of regional geological setting (Guillen et al. 2008). Moreover, the main limitation to the use of modeling software is that there are no clear guidelines for selecting a specific modeling method and algorithms details are not often freely available to public use (Natali et al. 2013).

The first consideration for 3D hydrogeological modeling is the availability of inputs to the modeling software in the appropriate format. Thus, the specific modeling method chosen will also vary based on defined inputs. Natali et al.(2013) presented various modeling approach and associated workflow depend on data availability such as data-free; sparse-data and data-dense. The sparse-data modeling method is the most frequently used because it allows the combination of field measurement and geostatistical tools to characterize subsurface hydrogeological setting efficiently.

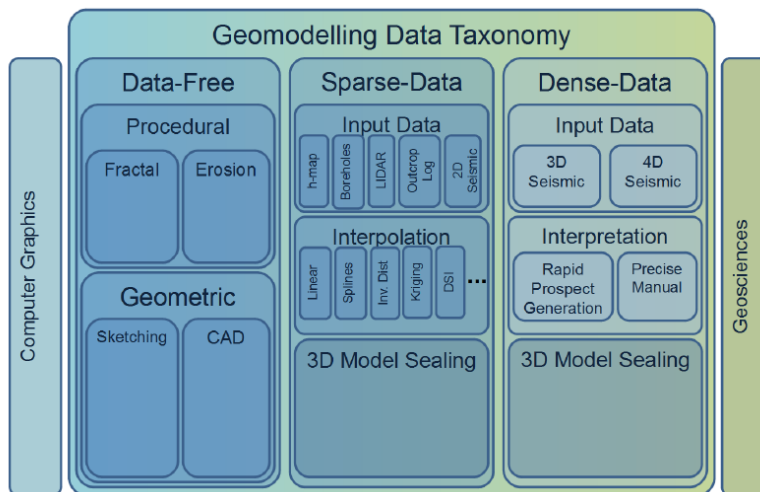


Figure 8. Types of modeling methods according to the type of data available and from which domain they originate (from Natali et al. 2013)

Three-D modeling and visualization offer numerous advantages when compared to the conventional way of using 1-D or 2-D methods such as; (Raju et al. 2015)

- Integration of data from various methods of investigation(geophysics, hydrogeology, hydrochemistry);
- Analysis and visualization of subsurface information;
- Coupling groundwater and surface water models.

5. Methodology

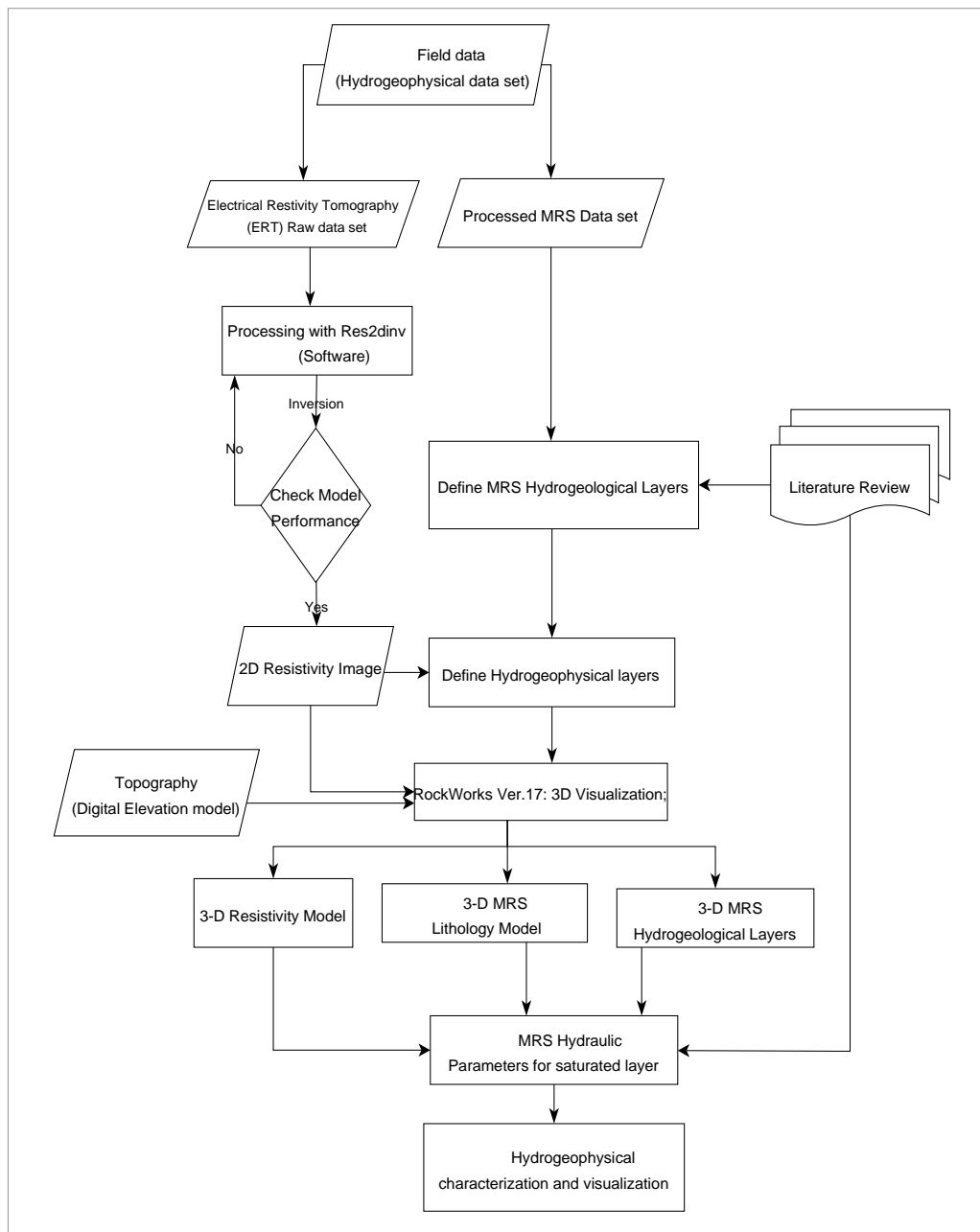


Figure 9. Methodology Flow chart diagram

For characterizing the subsurface hydrogeological structure of a region, it is necessary to collect and compile all relevant hydrogeological information from different sources at various scales and organize them into a unified structure which describes the knowledge and qualitative understanding of regional hydrogeological setting and properties which influence groundwater occurrence (Yao et al. 2015). This chapter discusses data sources, tools and methods used for preparing and processing the data to achieve the stated objectives and the workflow comprise:

- ◆ Analysis and processing of geophysical datasets to retrieve relevant hydrogeological parameters.
- ◆ Assemble all available datasets in an appropriate format to the modeling software.
- ◆ Characterize subsurface hydrogeological setting; 3D model block which depicts the spatial extent of hydrogeophysical layers and associated hydrogeophysical parameters.

5.1. Data Sources and formats

To characterize the subsurface hydrogeological setting of the region, it is crucial to have all data available in usable digital format for the modeling software. This section describes the type and sources of data used in this work.

5.1.1. Digital Elevation Models (DEM)

A Digital Elevation Model (DEM) of the earth's surface is essential for geological modeling, and they are used to represent the land surface of the model. The Digital Elevation Models are gridded representation of the surface of the earth where each pixel in the grid contains elevation value. A digital elevation model from Shuttle Radar Topographic Mission (SRTM) was selected to replicate the region's ground surface elevation. The SRTM DEM is currently distributed free of charge by USGS and can be downloaded from the website (<https://earthexplorer.usgs.gov/>). The SRTM Digital elevation model is disseminated in two different horizontal resolution such as; STRM 30m resolution and SRTM 90m resolution. The SRTM 30m was used because of its high resolution, and field measurement are not evenly distributed to replicate ground's surface model.

5.1.2. Geophysical datasets

In August of 2018, a team of University of Sciences in Wuhan, Hubei, China led by Prof. Li conducted geophysical survey to investigate geophysical properties which influence groundwater dynamic at Maqu sub-catchment. Thus, a total of fourteen (14) ERT data sets and eighteen (18) MRS survey points were obtained. The ERT measurement was conducted using two types of array configurations; Wenner and the dipole-dipole. The two configuration methods were adopted according to their capabilities to characterize vertical and horizontal subsurface heterogeneity respectively. Hence, for each surveyed line two types of surveyed profiles were obtained with 90 electrodes at 10 meter spacing between each electrode for a total length of 890 meters. The ERT raw data were obtained for further processing whereas MRS inversion results were made available by Dr. Jean Roy for further hydrogeological interpretation. The measurements location are shown in Figure 10.

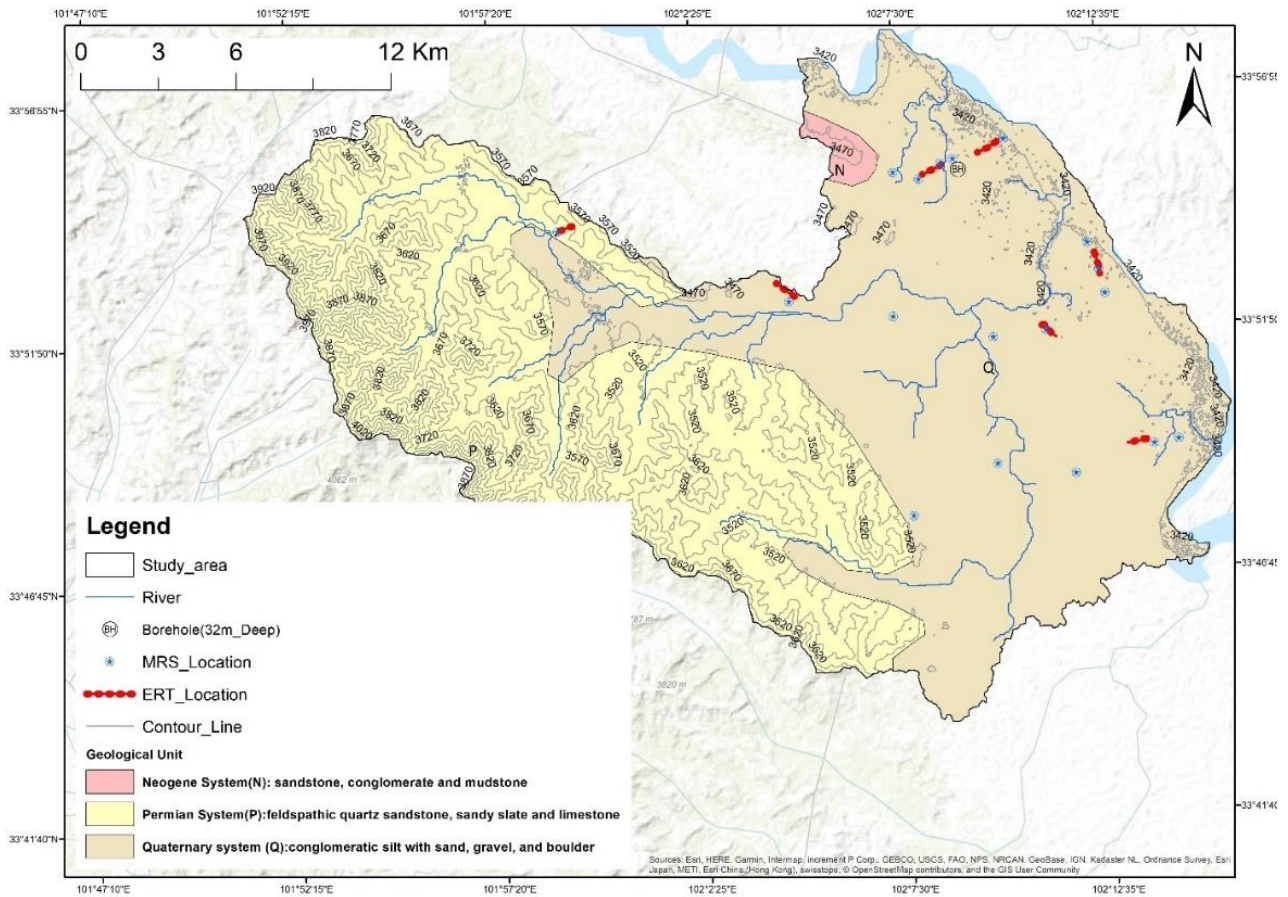


Figure 10. Field plan and location of ERT Lines, MRS detection loop.

5.1.3. Existing borehole logging

Hydrogeological characterization requires geological data in which the units can occur. Their topology is produced by compiling geological structure in correct and unique super-positional order. Gathered information on topological structure enables to define hydrogeological layers which are essential for constructing the hydrogeological model (Mathers et al. 2012). Borehole drilling is usually a conventional way for defining the lithological structure in which geological unit can occur. And information from borehole can be used to validate hydrogeological parameters derived from geophysical methods. The study area contains one existing borehole located at an elevation of 3385 m.a.s.l, and the groundwater level was reported to be at 12m below ground surface. Depth and lithology of the drilling are depicted in Figure 11.

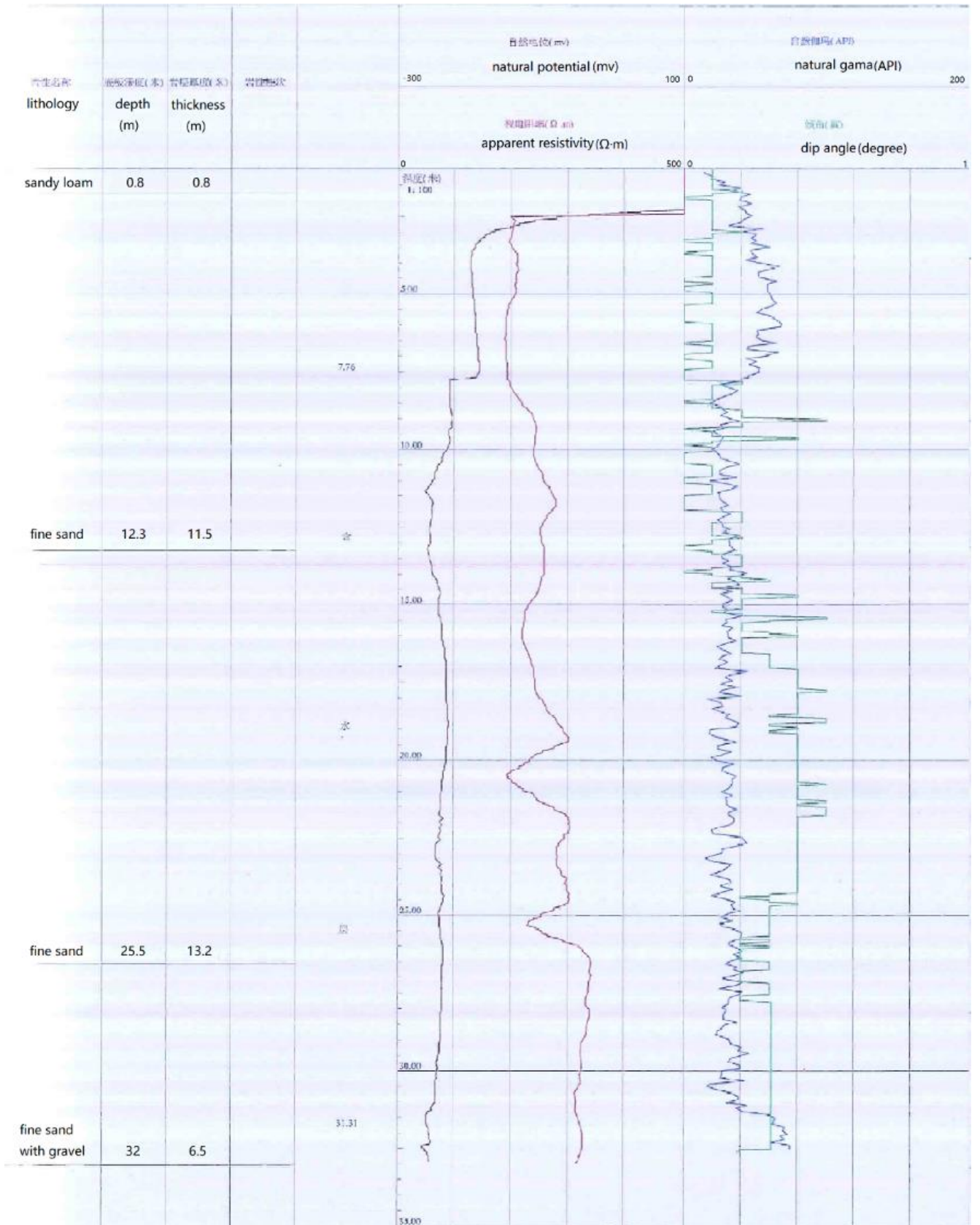


Figure 11. Existing borehole logging

Table 6 Data Source and Format

Source	Data Type	Acquisition Method	Information	Format
GROUND DATA	geophysical data sets	Nuclear Magnetic Resonance Sounding (NMR)	Free water content (%) and Decay time constants (milliseconds)	DAT.FILE
		Electrical Resistivity Tomography (ERT)	Apparent resistivity (Ohm. Meter),	WDA.FILE
Satellite data	DEM	Downloadable	SRTM 30m resolution (Topography)	ASCII.FILE

5.2. Data preparation

Data processing and analysis involves the following main steps: (1) Processing of ERT data set to retrieve 2D subsurface resistivity image at each surveyed line ; (2) Create ground surface grid model using Digital Elevation Model (DEM) for constraining solid model to ground surface elevation ;(3) Define MRS hydrogeological layers and associated lithological properties using qualitative and quantitative analysis of MRS hydrogeophysical parameters ; and (4) Transform all available datasets into appropriate format for modelling software.

5.2.1. ERT data processing

The ERT field measurements were obtained and processed using RES2DINV, ver. 4.8.6 program. This program was used because it was made freely available and it can support different types of data format, depending on the type of array configuration used for field data acquisition. This program was designed to invert the “apparent resistivity” from electrical tomography surveys into two dimensional (2D) subsurface image of “True resistivity” in an automatic manner with minimum input from the user. The inversion program determines the resistivity model that approximates the best fit with a minimum error between measured and calculated value. This is a simultaneous process which involves two steps such as forward and inverse modeling.

The default parameters were used for model discretization, which subdivides the subsurface into some rectangular blocks and the arrangement is loosely tied to the distribution of measured value. The cell-based method which is most frequently used in inverse modeling was applied. This method is particularly useful because it takes into account both lateral and vertical changes within the cells whereas the size and position of the cells remain fixed. The finite difference method was used for the forward modeling calculation, and the inversion routine was performed using robust inversion or blocky (L1-norm) method because it is reported to be less sensitive to noise data.

Before carrying out inversion, field data were converted into an appropriate format (.DAT) for inverse modeling software using "Converter.exe." Each transect was converted and made ready for inversion. The practical routine was to import the file of a particular transect and display into inversion software to pick out bad data points (Noise data) which are occurring during field data acquisition due to two types

of errors such as Systematic or Random error. This was achieved in two steps such as; pre-processing and pre-inversion. Pre-processing was conducted using RES2DINV visual interpretation tool (pseudo_section) to manually remove bad data points that appeared to be extremely outside of normal range (Figure 12). After data filtering, a pre-inversion was executed, and the magnitude of error between measured and calculated value was minimized where necessary by adjusting the filter threshold to remove scattered points using error distribution bar as shown in Figure 15.

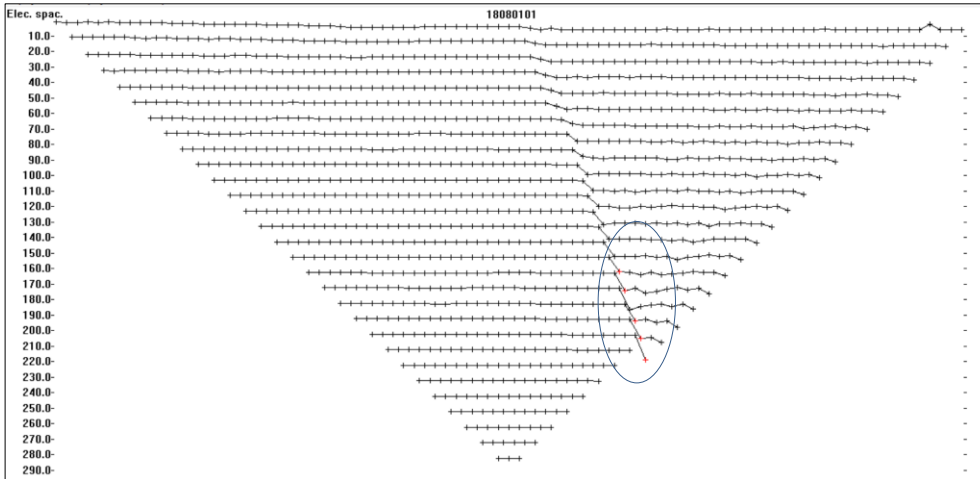


Figure 12. Example of data scatter before noise data rejection

Table 7 ERT Line information before and after editing

ID	Configuration	Line length(m)	Total raw points	Points after editing
	Wenner	890	1305	848
Line1	Dipole_Dipole	890	1305	1290
	Wenner	890	1305	1303
Line2	Dipole_Dipole	890	1305	1261
	Wenner	890	1305	1271
Line3	Dipole_Dipole	890	1305	1270
	Wenner	890	1305	1305
Line4	Dipole_Dipole	890	1305	1305
	Wenner	810	1080	1080
Line5	Dipole_Dipole	810	1080	1080
	Wenner	810	1080	1080
Line6	Dipole_Dipole	810	1080	1080
	Wenner	810	1080	1080
Line7	Dipole Dipole	810	1080	1080

The inversion results for each profile is presented into three sections; the top section is showing raw data, the middle section shows the forward model solution and the bottom section shows the inversion model. Figure 13 shows a screenshot of inversion with Res2din.

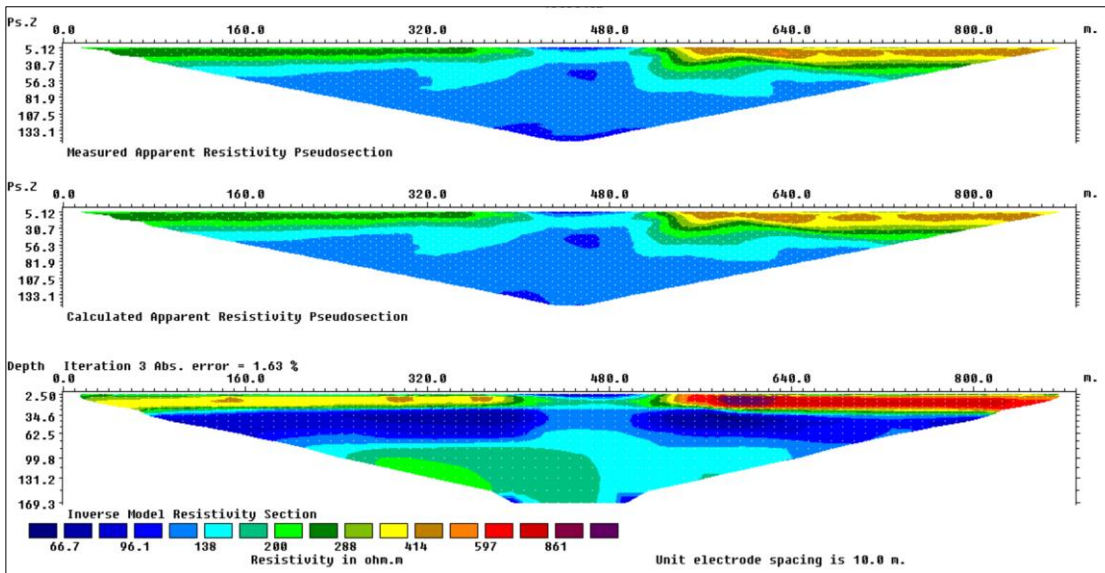


Figure 13. Example of Screenshot for inversion results with Res2dinv software

Then, the final inversion was performed, the model output was accepted at the iteration beyond which the magnitude of Root Mean Square (RMSE) does not change significantly. This was achieved between 3rd and 5th iterations, and this resulted in a 2D image of subsurface resistivity distribution in terms of distance along the surveyed line versus investigated depth. To combine both advantages of two different array configurations, the final inversion results for each surveyed line were visually compared for the quality control. Figure 14 shows the flowchart methodology for ERT data Processing. Coordinates of electrodes along the surveyed line were obtained and incorporated in the inversion where necessary for quality control, but it was not used as part of the 2D inversion results because all profile present a slight change in topography relatively to the length of the line.

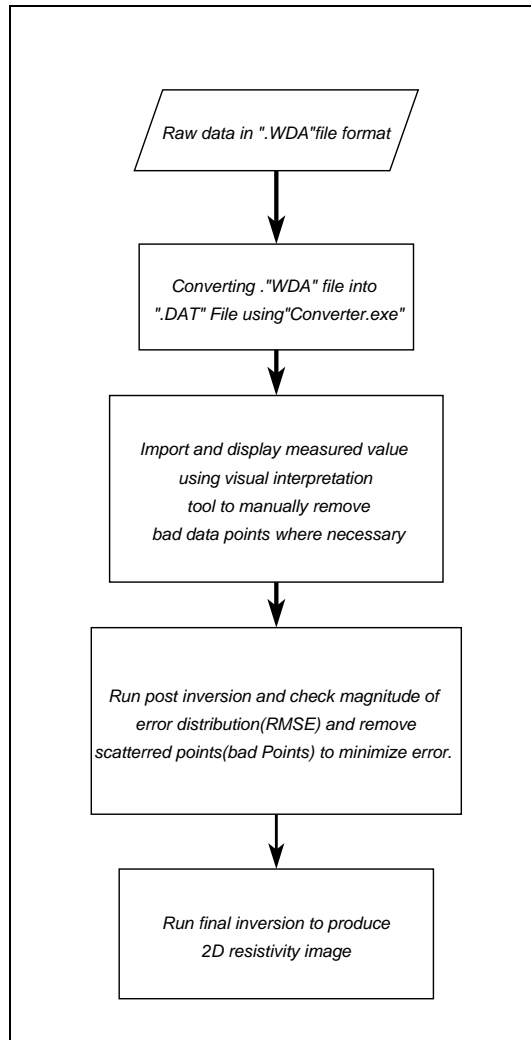


Figure 14. 2D Resistivity processing flowchart

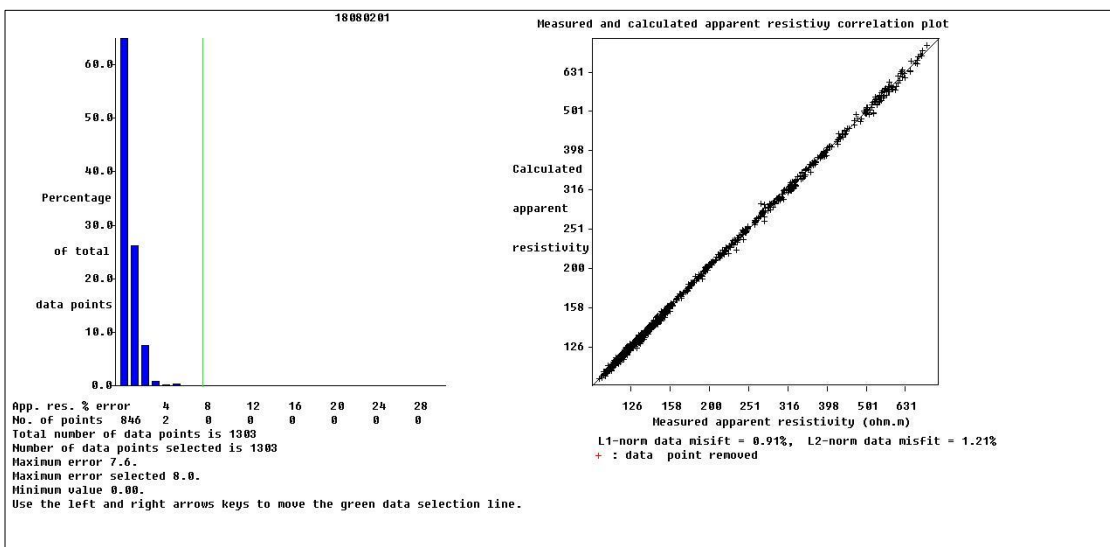


Figure 15. Data removal filter during pre-inversion process (ERT Line 2, Wenner array configuration).

To plot 2D image, the inverse model section for each profile was exported using surfer format tool and then gridded using Surfer® software package version 16.0. A standardized color file to represent resistivity variation (Ohm.m) was applied for better visualization of resistivity patterns, and the results are presented in section 6.2.

5.2.2. MRS data set

Magnetic Resonance Sounding (MRS) was conducted in this study to define aquifer geometry and estimate subsurface hydraulic properties (Both storage and flow parameters). The MRS-inverted parameters were obtained from Dr. Jean Roy who processed the data using Samovar version 11.6 with a smooth Singular Value Decomposition (SVD) guided procedure, and more details can be found in Legchenko et al. (2017). The inverted plots from MRS signals comprise sounding curves which depict amplitude of relaxation signal as function of Pulse moment. The interpreted geophysical curves include: free water content in percentage as the function of depth, relaxation time constants in milliseconds (ms) versus depth, and graph depicting resolution of MRS signals as a function of depth, which shows the maximum resolution depth at which inversion results can be certain. The maximum resolution depth is always smaller than the sounding investigation depth (Mazzilli et al. 2016). The summary of MRS inversion curves (Free water content and decay time constant) are presented in section 6.2.

Table 8. Summary of the MRS investigations. Field camp: Field Campaign. S/N: Signal-to-noise ratio. EN/IN: External noise to instrumental noise ratio.

ID	Field comp.	S/N	EN/IN	Geomagnetic field (nT)	Loop shape(Side)
MRS1-1	01-Aug	11.35	7.4	52624.41	Square (150m)
MRS2-1	02-Aug	19.18	3.3	52624.41	Square (150m)
MRS3-1	03-Aug	26.57	4.5	52624.41	Square (150m)
MRS3-2	03-Aug	18.69	6.6	52624.41	Square (150m)
MRS4-1	04-Aug	13.74	8.3	52624.41	Square (150m)
MRS4-2	04-Aug	0.45	164.1	52624.41	Square (150m)
MRS5-1	05-Aug	34.46	4.6	52624.41	Square (150m)
MRS5-2	05-Aug	2.68	54.6	52624.41	Square (150m)
MRS6-1	06-Aug	1.38	44.6	52617.37	Square (150m)
MRS7-1	07-Aug	32.65	7.6	52617.37	Square (150m)
MRS7-2	07-Aug	15.61	15.6	52605.63	Square (150m)
MRS8-1	08-Aug	22.66	4.0	52605.63	Square (150m)
MRS8-2	08-Aug	0.8	99.1	52605.63	Square (150m)
MRS9-1	09-Aug	5.21	34.5	52605.63	Square (150m)
MRS9-2	09-Aug	1.86	53.7	52593.90	Square (150m)
MRS10-1	10-Aug	1.97	45.5	52617.62	Square (150m)
MRS11-1	11-Aug	6.18	5.6	52659.62	Square (150m)
MRS11-2	11-Aug	1.85	52.6	52605.63	Square (150m)

5.2.3. Model extent and digital elevation model

The fact that the study area is undersampled, even with an unoptimized location of field measurement. The modeling extent was restricted to maximum and minimum coordinates of geophysical measurement as depicted in Figure 16.

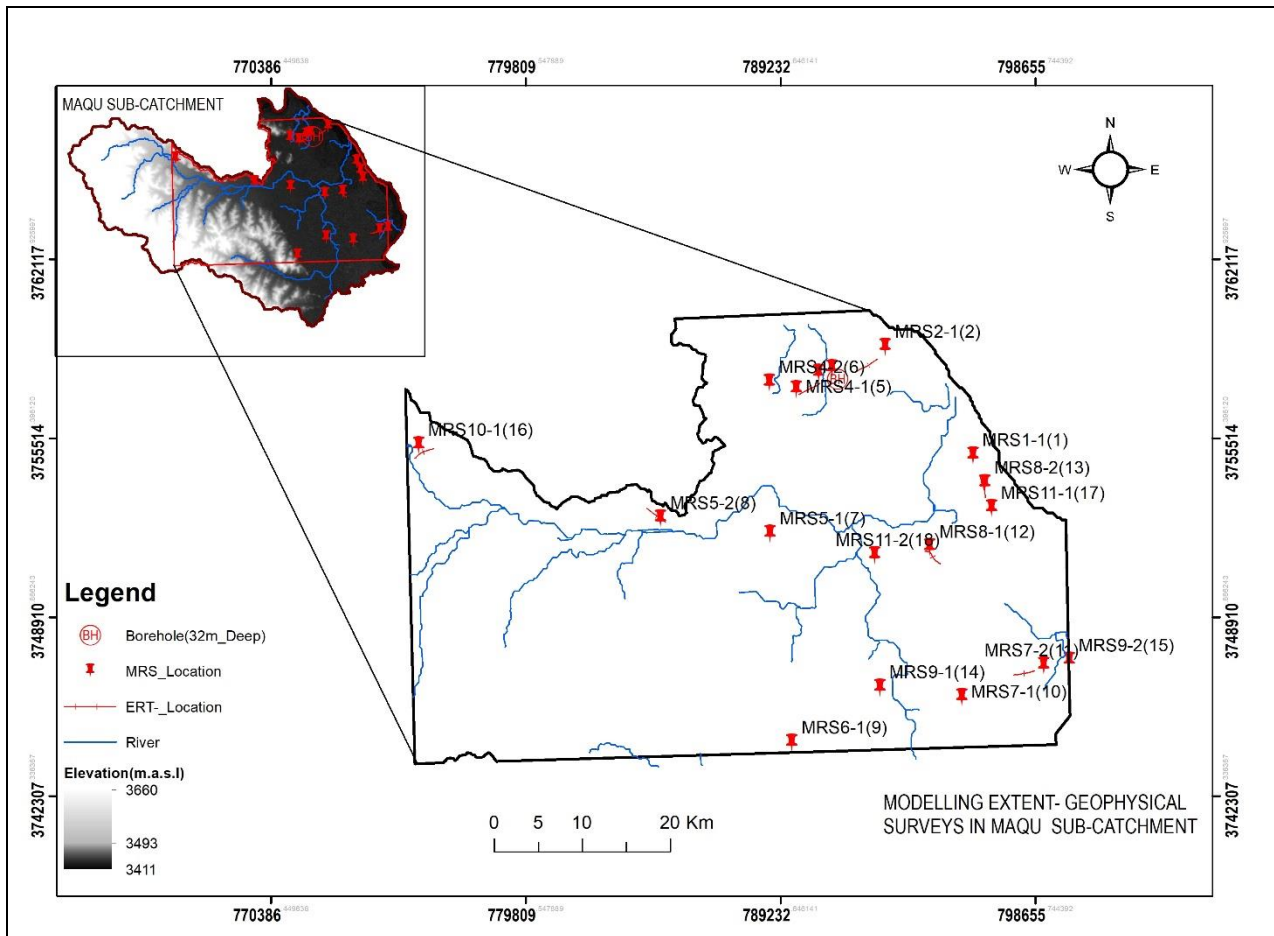


Figure 16. An overview of modeling extent with a location of geophysical survey and existing well logging

A digital elevation model from Shuttle Radar Topographic Mission (SRTM) of 30×30 m horizontal resolution was used to replicate the solid model's ground surface. ArcGIS software ver.10.5 and Microsoft Excel were used to transform DEM into the acceptable format by the modeling software. The used geographic coordinates system to build 3D grid surface model is UTM WGS84-Zone 47N, and the grid surface model was restricted to the maximum, and minimum coordinates of field measurement as shown in Figure 16 and the output model dimensions were adjusted to $30 \times 30 \times 0.5$ m and $30 \times 30 \times 10$ m grid resolution to constrain 3-D lithology, 3D hydrogeophysical mode, and 3-D resistivity model respectively.

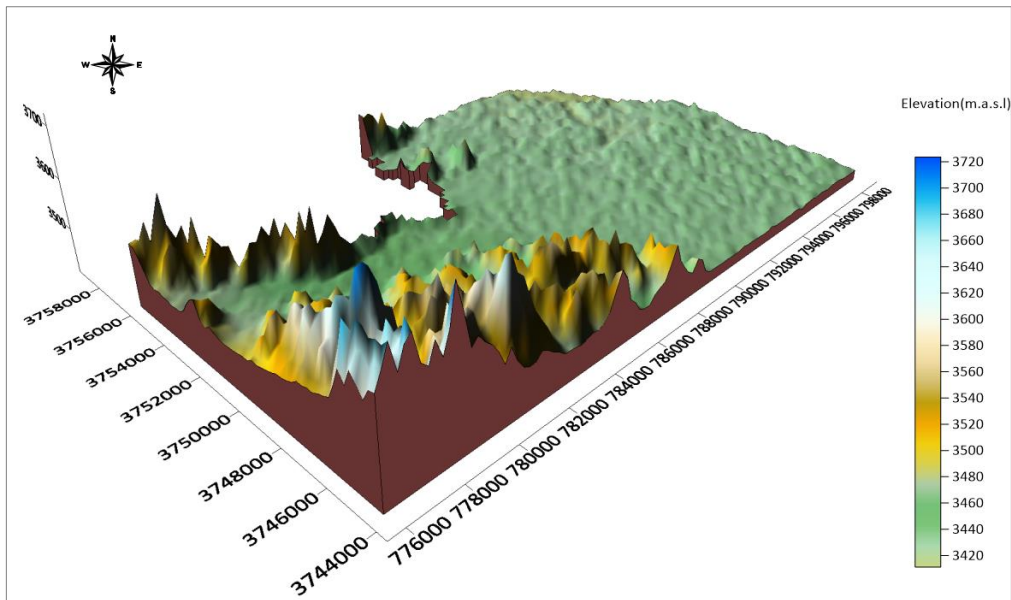


Figure 17. Model extent: 3-D Digital elevation model

5.3. Software consideration

Geographical Information System (GIS) tools are widely used for hydrogeological model conceptualization and groundwater modeling due to their capabilities of integrating large volume of datasets and allowing to characterize spatial relationships between subsurface geological features in two or three dimensions (Trabelsi et al. 2013). Thus, It is essential to select an appropriate software package based on both desired output as well as the available input data. In this work, RockWorks, vers. 17 was chosen because it is a GIS-based software package and it is capable of analyzing and visualizing geophysical, geological and stratigraphical, hydrogeological and borehole data. And multiple interpolation algorithms are available within this program which facilitates complex analysis of spatially distributed datasets. Moreover, RockWorks can produce several types of images of modeled subsurface formations, including 3D solid model, fence diagrams, cross sections, profiles, and 2D maps. Excel spreadsheet was used to create and manage the subsurface hydrogeophysical database and Digital elevation model data set because it can handle large datasets and it has the capability to interface easily with RockWorks.

5.4. Three-dimensional modeling and database structure

Actual measurements of subsurface properties are very scattered and limited to 1D or 2D measurement. Also, those properties do not have a normal distribution which makes difficult for their interpretation and presentation even at a small catchment scale. In this work, 2D resistivity image was constructed using RES2DINV software package, and 1D MRS hydrogeological profiles were obtained. The 3D visualization is used to integrate them.

A mathematical way of expressing the spatial distribution of these parameters must be found. Thus, inverse distance weighting and lateral blending techniques were used for interpreting resistivity value and providing a link between MRS hydrogeological layers, respectively. These methods were selected because they are particularly useful to interpolate stratiform data

The 2D resistivity profiles and MRS hydrogeophysical properties were transformed into the appropriate database structure, which complies with the modeling software. The final 2-D resistivity profile for each line was transformed into data points (x, y and z, and resistivity record) and the database was created using excel sheet. Then, imported into the Rockworks under geographic coordinate system UTM WGS84-Zone 47N. Afterwards, the 3D solid model was built using anisotropic inverse-distance weighting technique (IDW-Anisotropic). This algorithm enables the program to use the closest control points in each sector around the node, and a voxel node value is assigned based on the weighted average of neighboring data points. Then, the value of each data point is then given based on the inverse distance from the voxel node value. Declustering, smoothing, super surface were also applied in the modeling for filtering. After interpolation, the solid model was clipped to study area.

The lithology model of the study area was constructed using lithology-solid modeling option available in RockWorks. First, the MRS Hydrogeological layers were constructed by combining MRS free water content and decay time constant. Using the excel sheet associated lithology were assigned using petrophysical information (See Table 4). These layers were stored in the lithology-type table of RockWorks database. This table contains information about rock material, assigned pattern or color, and the order in which the layers are occurring from ground surface to MRS depth of investigation. A unique numerical identifier (G-value) was assigned for each lithology type, and this value has been used to interpolate each lithology type and provide the link between MRS 1D profiles. The lateral blending interpolation technique was used to create the 3D solid lithological model. Then, the model was clipped to the study area boundary, and the grid surface model was used to replicate the solid model ground’s surface elevation.

Table 9. Rockworks Lithology type table

G-Value	Keyword	Pattern	Fill Percent	Density	Show in Legend
1.0	Clayey Sands or Very fine Sand		100	1.0	<input checked="" type="checkbox"/>
3.0	Coarse and gravely sands		100	1.0	<input checked="" type="checkbox"/>
2.0	Fine Sands		100	1.0	<input checked="" type="checkbox"/>
4.0	Gravels		100	1.0	<input checked="" type="checkbox"/>
6.0	Less weathered Rock		100	1.0	<input checked="" type="checkbox"/>
5.0	Sand Clayey		100	1.0	<input checked="" type="checkbox"/>

Table 10. The input data of 3-D lithology, 3-Resistivity Model and 3-D hydrogeophysical model

Data	Type	Details	Source
Geophysical Survey	Coordinates	UTM WGS 1984 Zone 47N	Field measurement
	MRS Lithological discription	Rock Composition	
	MRS hydrogeological layers	thickness(m)	
	Resistivity	2D ERT records	
Shapefile	Model extent	Digitization	
DEM	SRTM 30m	30m resolution	Downloadable

6. Results and Discussion

This section discusses the results obtained in this work following the data and methods described in section 5.

6.1. 2D ERT inversion results

The 2D inverted resistivity profiles are presented with some metadata that can assist in the interpretation: i) logarithmic color scale, which depicts the variation of resistivity along the profile and associated values, ii) depth of investigation and length of the profile (in meters). Table 11 shows the number of iterations and length of each profile, which varies from 810 to 890m, depends on the number of electrodes used, and the depth of investigation is stretched from ground surface up to the maximum of 150m deep. The root mean square between the resistivity model and the field apparent resistivity range from 0.91% to 7.6% as shown in Table 11. The resistivity value range from very electrically conductive to high resistive medium. Generally, ERT inverted profiles show a shallow and deep electrically resistive layer and the electrically conductive layer in the middle. For practical interpretation, ERT profiles can be sorted into depth-wise of resistivity value as follows:

- ❖ Profiles with top thin surficial layer characterized by resistivity patterns $>200 \Omega.m$, underlain by layer with low resistivity value $<150 \Omega.m$, followed by a thin deeper layer with resistivity value $>150 \Omega.m$ (See Figure 18; Figure 19 and Figure 23).
- ❖ Profiles with top surficial thin layer characterized by resistivity value $>200 \Omega.m$ but with some local interruption, underlain by a thick layer with resistivity value $<150 \Omega.m$, and finally, a deeper layer with resistivity value $>150 \Omega.m$ and $<250 \Omega.m$ but with some interruption (see Figure 20 and Figure 22).
- ❖ Profiles with a thin surficial layer with relatively low resistivity $<150 \Omega.m$, followed by a layer with high developed resistivity patterns up $1500 \Omega.m$ (see Figure 24).
- ❖ ERT Line 4 shows resistivity value $<150 \Omega.m$ with slight variation along the profile and can be interpreted as a single layer (See Figure 21).

Table 11. ERT surveys with root mean square below than 8% after inversion

Profile	Array configuration	Length(m)	Data Points	RMS Error (%)	Number of iterations
Line1	Wenner	890	848	0.91	3
	Dipole Dipole	890	1290	7.63	4
Line2	Wenner	890	1303	1.28	3
	Dipole Dipole	890	1261	2.1	4
Lin3	Wenner	890	1271	0.61	3
	Dipole_Dipole	890	1270	1.56	3
Line4	Wenner	890	1305	0.98	5
	Dipole_Dipole	890	1305	2.3	3
Line5	Wenner	810	1080	1.64	3
	Dipole_Dipole	810	1080	1.88	4
Line6	Wenner	810	1080	2.4	3
	Dipole_Dipole	810	1080	2.5	4
Line7	Wenner	810	1080	1.61	3
	Dipole_Dipole	810	1080	3.3	3

6.2. Comparison of MRS and ERT outputs

To obtain a complete hydrogeophysical interpretation from both hydrogeophysical tests, a comparison between ERT and MRS outputs is presented in this section. To facilitate the comparison, each ERT inverted profile was compared to the nearest MRS profile. As indicated by MRS hydrogeophysical curves, the MRS free water content and decay time constant for each sounding vary with depth indicating the presence of diverse lithology, as well as the inverted resistivity profiles, present varying patterns with depth. Thus, interpretation is needed to provide the link between the two sources of hydrogeophysical data.

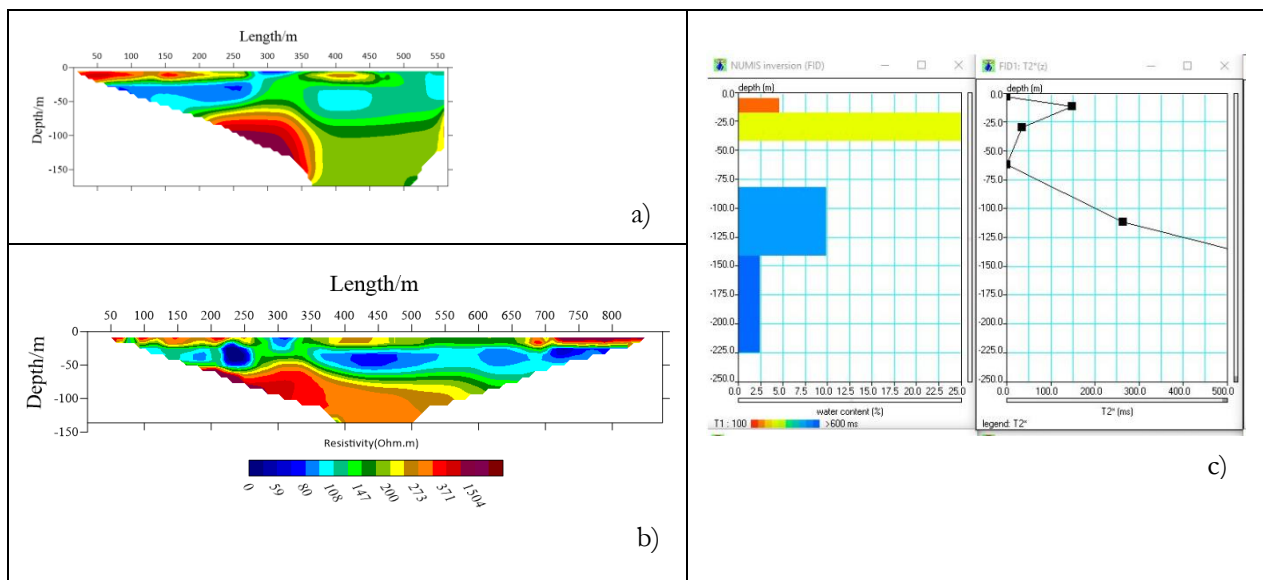


Figure 18. a) ERT Line1 Wenner configuration, b) ERT Line1 Dipole Dipole Configuration, C) MRS 8-2: Water content and T2* versus depth.

MRS8-2 was conducted within a few meters at the end of ERT line1. Three hydrogeophysical layers can be sorted by referring to Figure 18 ; A top layer with resistivity value greater than 200Ω-m stretching from ground surface to 20m deep but with local interruption in the middle of surveyed line and average water content reaching 3.5%, followed by a low resistive layer <150 Ω-m lies approximately between 20 to 60m deep and average water content reaching 15%, and finally a deep layer with developed electrical resistivity > 150 Ω-m and low MRS water content reaching 5% and a thickness stretching from 60m up to investigated depth.

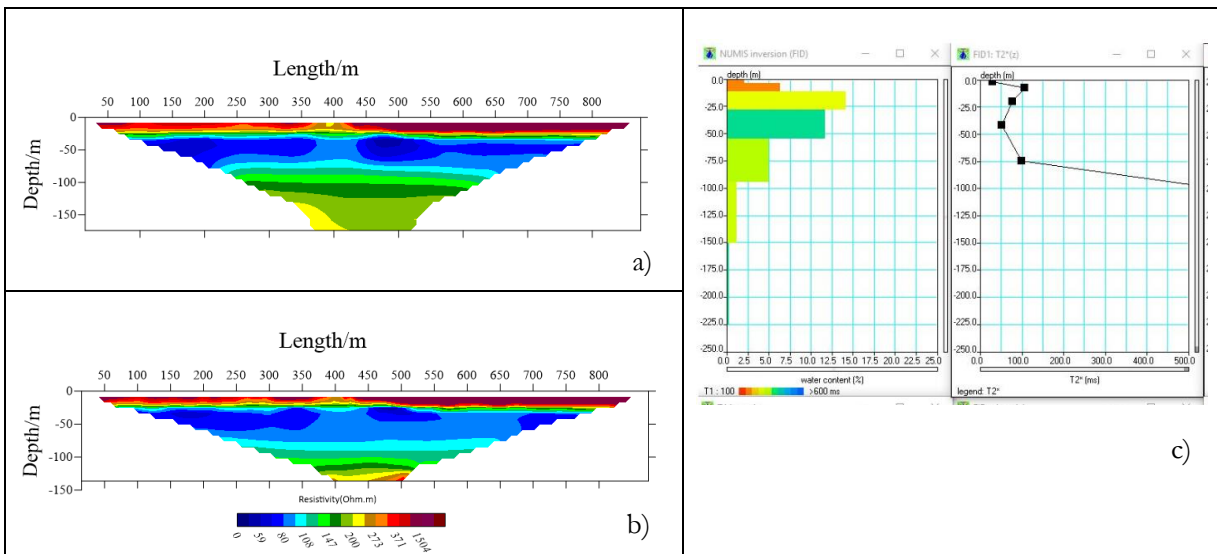


Figure 19 a) ERT Line2 Wenner configuration, b) ERT Line2 Dipole-Dipole Configuration, C) MRS 2-1: Water content (%) and T2* versus depth

As shown in Figure 19 three layers can be sorted ; top layer with resistivity value greater than 200Ω-m stretching from ground surface up to 20m deep and average water content reaching to 5% can be assigned, followed by a low resistive layer <150 Ω-m with thickness varies between 20m to 60m deep and average water content reaching 13 %, and finally a deep layer with less developed resistivity >150 Ω-m and average water content 5% stretching from 60m up to investigated depth.

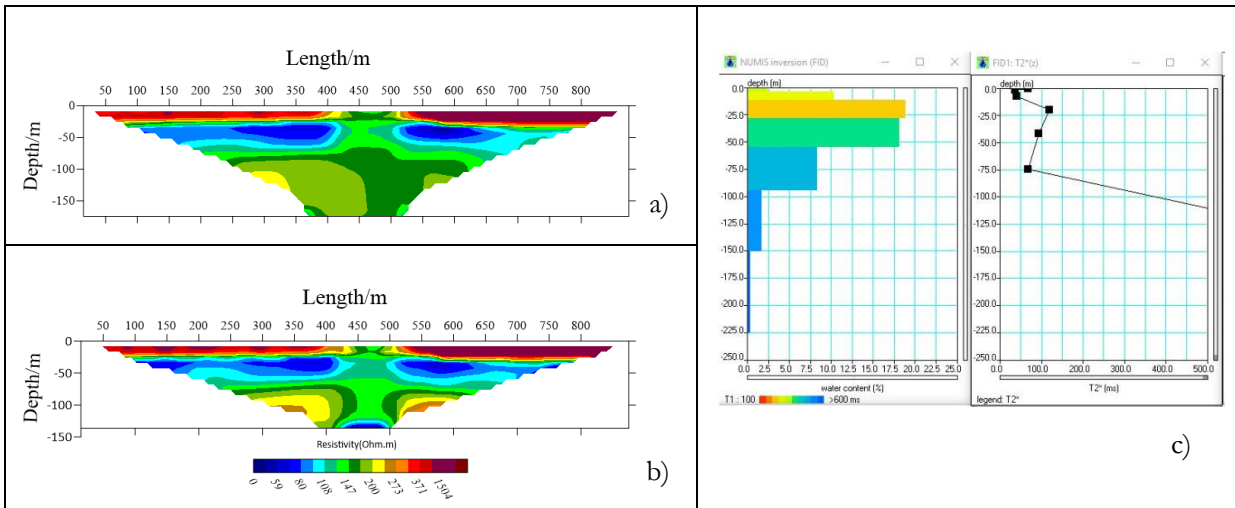


Figure 20 a) ERT Line3 Wenner configuration, b) ERT Line3 Dipole Dipole Configuration, c) MRS 3-2: Water content (%) and T2* versus depth.

MRS3-2 was conducted proximally to ERT line 3. As depicted in Figure 20 ; three depth-wise layers can be interpreted : The topmost layer stretching from ground surface to 20m deep with resistivity value $>200\Omega\text{-m}$ and average water content reaching 8% , followed by a low resistive layer $<150\Omega\text{-m}$ with an approximative thickness of 40m varies from 20 to 60m deep and water content reaching 17%, and finally with a less developed resistivity layer $>150\Omega\text{-m}$ stretching from 60m up to investigated depth and MRS water content reaching 6% can be assigned.

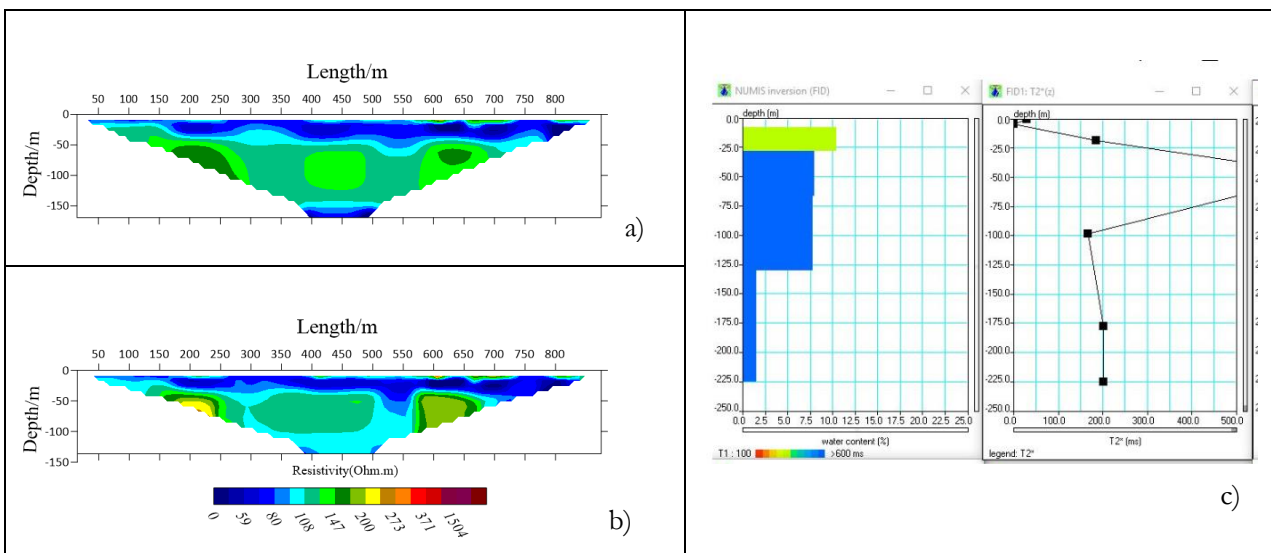


Figure 21 a) ERT Line4 Wenner configuration, b) ERT Line4 Dipole Dipole Configuration, c) MRS 5-2: Water content (%) and T2* versus depth.

MRS5-2 was conducted near to ERT Line 4, as shown in Figure 21, the resistivity pattern represents low value, and are not significantly change compared to other profiles, even MRS water content does not vary significantly with depth. Therefore, one hydrogeophysical layer can be assigned with resistivity value $<150\Omega\text{-m}$ and average water content of 6%.

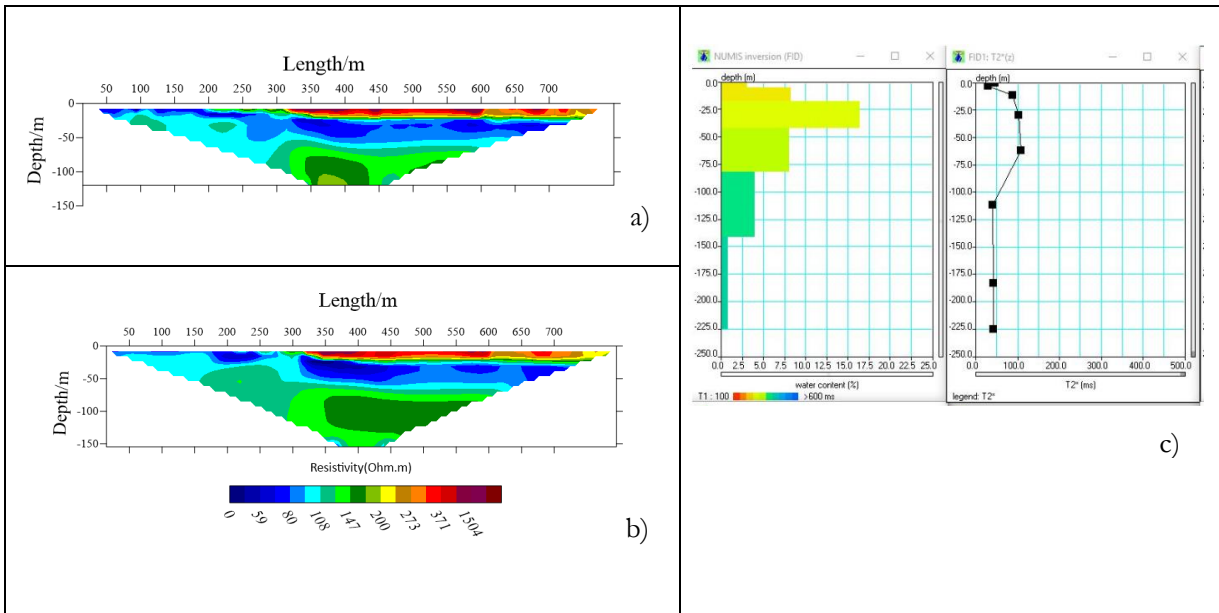


Figure 22 a)ERT Line5 Wenner configuration, b) ERT Line5 Dipole Dipole Configuration, C) MRS 8-1: Water content (%) and T2* versus depth.

ERT Line 5 was carried out in the vicinity of MRS8-1, as shown in Figure 22 three depth-wise hydrogeophysical layers can be interpreted : a thin top layer with resistivity value $> 200\Omega\text{-m}$ but with interruption at the beginning of the line and MRS free water content reaching about 7%, stretching from ground surface to 20m deep, followed by a low resistive layer extending from 20m up to 60m deep with resistivity value $< 150\Omega\text{-m}$ and average MRS free water content of 16%, and finally a deep layer with less developed resistivity $> 150 \Omega\text{-m}$ but $< 250 \Omega\text{-m}$, with MRS free water content reaching 7% and thickness stretching from 60m deep up to investigated depth.

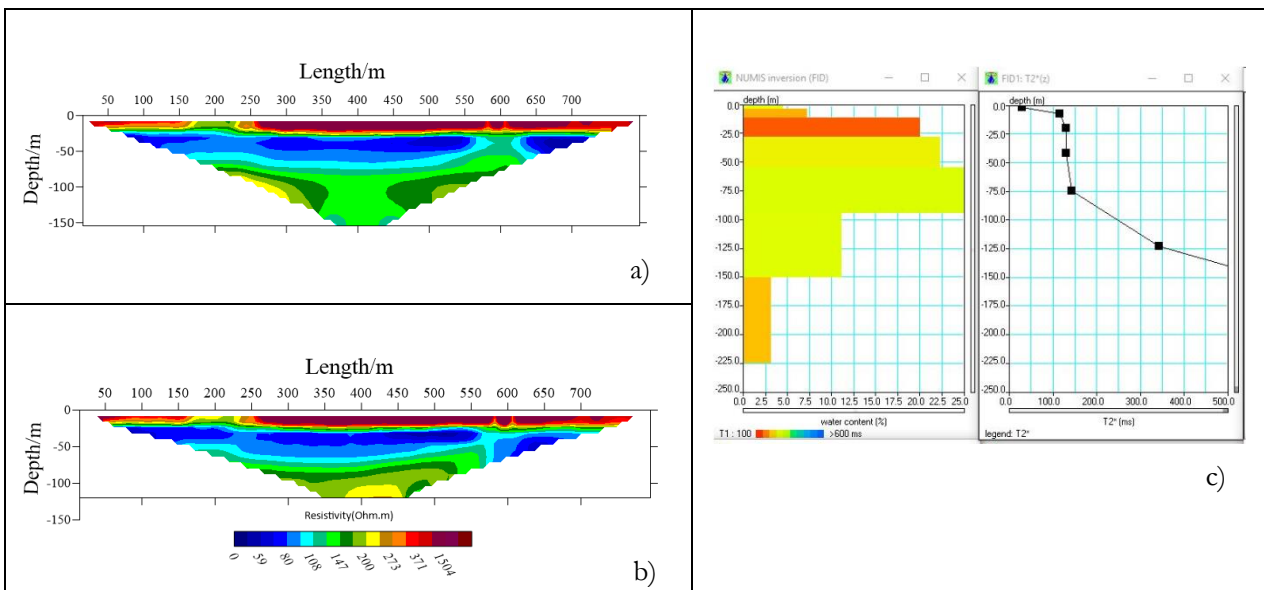


Figure 23 a) ERT Line6 Wenner configuration, b) ERT Line6 Dipole Dipole Configuration, C) MRS 7-2: Water content (%) and T2* versus depth.

ERT Line6 was performed near to MRS 7-2. Figure 23 shows three depth-wise resistivity layers : topmost thin layer stretching from ground surface to 15m deep with resistivity value $> 200\Omega\text{-m}$ and MRS free water content reaching 7%, followed by a low resistive layer <150 extending from 20m up 60m depths with an average water content of 25%, and lastly a deeper layer extending from 60m up to investigated depth with resistivity value of greater $> 150\Omega\text{-m}$ and an average water content of 10%.

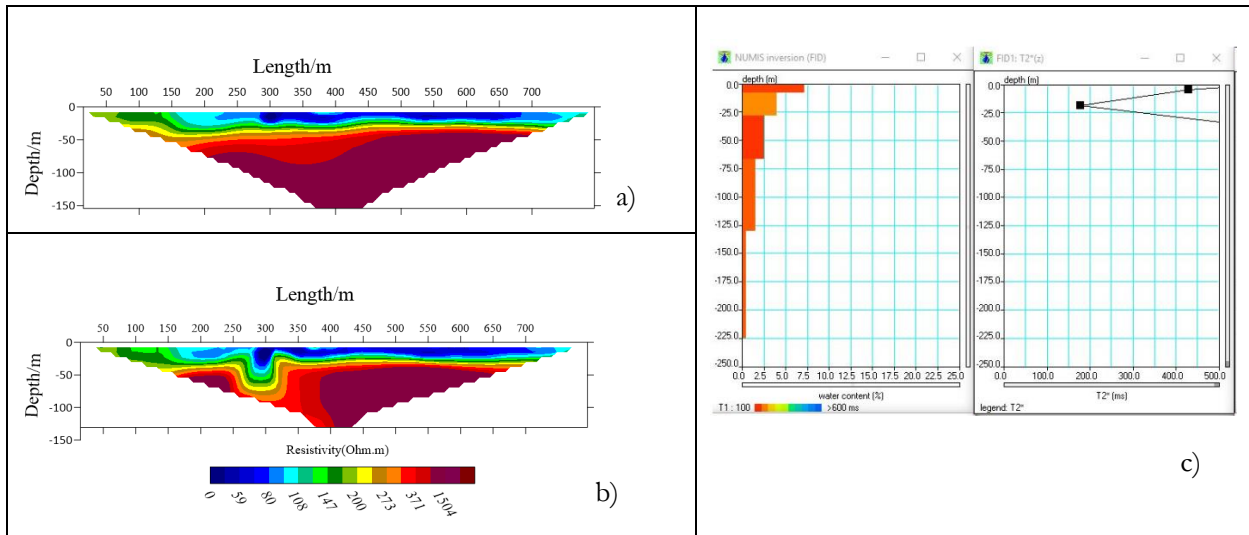


Figure 24 a) ERT Line7 Wenner configuration, b) ERT Line5 Dipole Dipole Configuration, C) MRS 8-1: Water content (%) and T2* versus depth.

ERT Line 7 was performed near to MRS 10-1. As illustrated by Figure 24, two hydrogeophysical layers can be interpreted : the topmost thin layer stretching from ground surface up to 20m deep with less developed resistivity $< 150\Omega\text{-m}$ and average MRS water content reaching 7% ; followed by a thick deep layer extending from 20m up to depth of investigation with high developed resistivity up to $1500\Omega\text{-m}$ (Consolidated sediment) and low MRS free water content $< 3\%$. which reflect an increased level of compaction

In general, the applied hydrogeophysical methods helped to estimate location of soil water-bearing formations through low resistivity patterns $<150\Omega\text{-m}$ which are associated with an increase of MRS water content, except for ERT Line-4 and MRS 5-2 (Figure 21) which present low electrical resistivity with slight variation compared to other profiles and this can reflect anomalous in subsurface conditions (Wet clay). It is important to note that ERT Line-4 and MRS5-2 were implemented over the area, which is the interface between mountainous areas and the third terrace (i.e. close to the drainage corridor).

6.3. Subsurface hydrogeophysical characterization

6.3.1. 3-D Resistivity modeling and interpretation

To visualize the spatial variation of electrical resistivity over the study area, a reconstruction process was made in the form of a solid model using RockWorks17 software by RockWare. The spatial variation of resistivity can be visualized using visual interpretation tools of the modeling software. Then, from its spatial variation and other supporting information underground condition can be estimated such as thickness of hydrogeological unit, groundwater presence through low resistivity and other relevant information.

A 3D visualization model using the output from the 2D resistivity value was built under geographic coordinates WGS84 System, UTM Zone 47N and presented in Ohm-meters. RockWorks Utilities tool was used to import and create database that contains field measurement locations and corresponding true resistivity values. Once inputted, the project's extension was restricted to field measurement location, giving project dimensions. 3-D solid modeling can take some time depends on model resolution applied. The finer the resolution, the longer the time it takes to construct the model. Nevertheless, the finer resolution does not reflect real distribution of field measurements because it takes an average over a large model cell.

The model resolution of 30X30X10m was used, and resistivity distribution was spatially analyzed by data interpolation(X and Y coordinates, Z elevation and resistivity value) using inverse distance weighting (IDW)-anisotropic technique available in RockWorks,17. This interpolation algorithm is particularly useful to interpolate data which are in stratiform deposits. But, this interpolation algorithm has the drawback of averaging data value by increasing and decreasing low and high value respectively. The distribution and frequency of 2D resistivity value from the inversion of 2D ERT profiles are depicted in Figure 25, and the resulting 3-D model as presented in Figure 26.

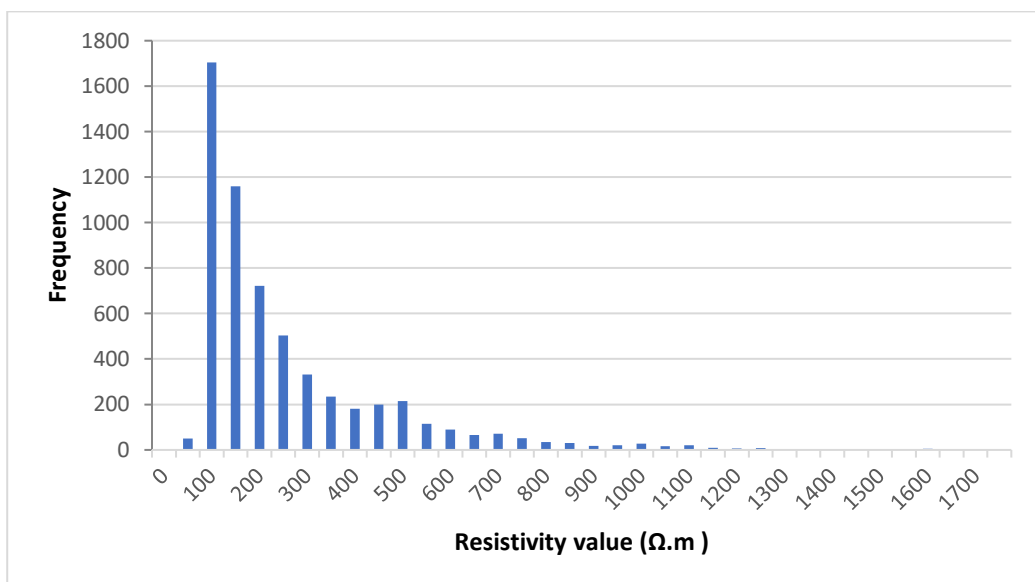


Figure 25. Frequency distribution of 2D resistivity (true resistivity) value

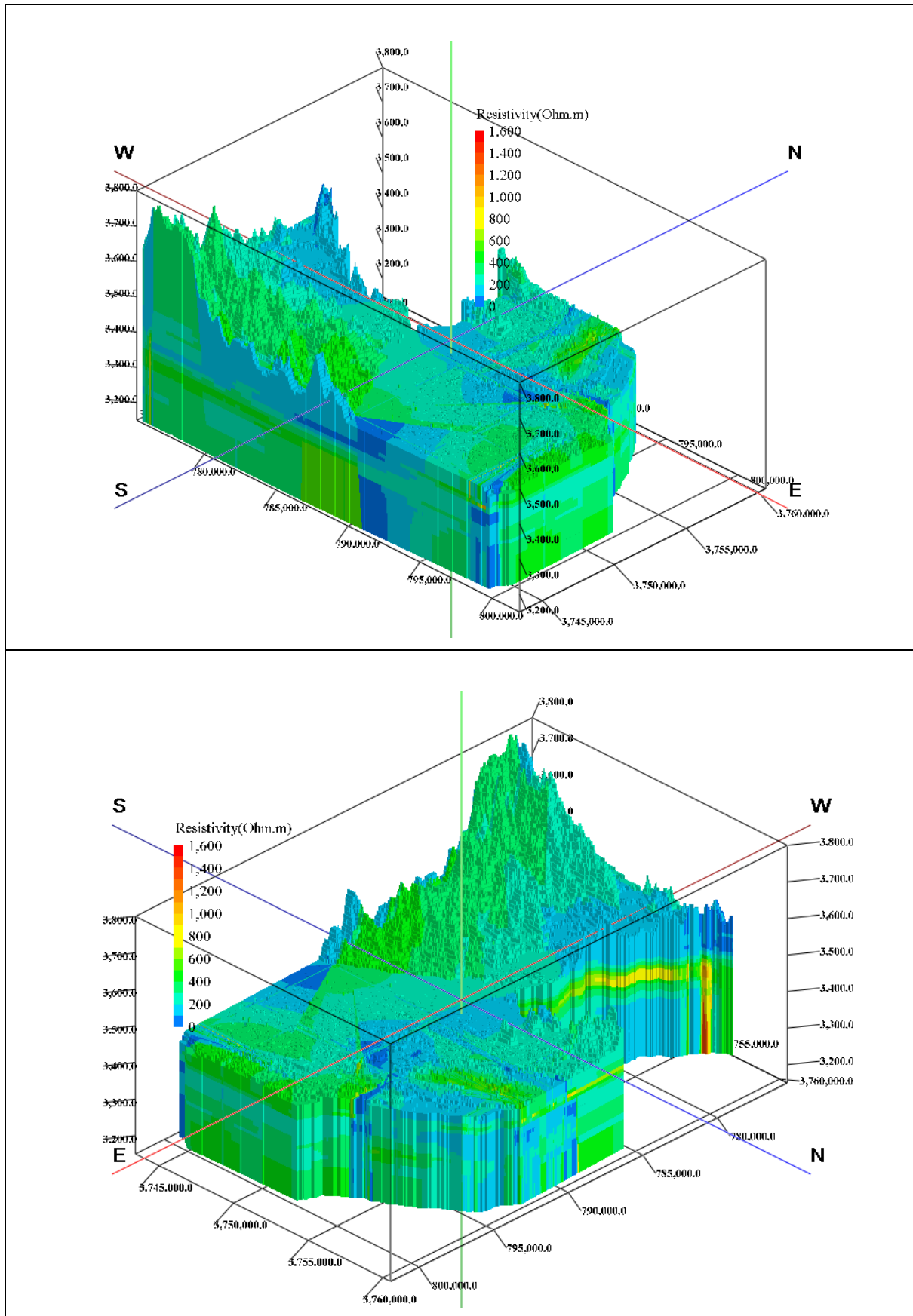


Figure 26 3-D visualizations of resistivity patterns: Vertical exaggeration is 20

Figure 26 shows a spatial variation of resistivity over the study area and by visual interpretation two components can be estimated such as; plain and mountainous components. A plain component can be sorted into three depth-wise resistivity patterns with a top electrically resistive layer $> 200 \Omega.m$ which could be explained by the degree of soil saturation but with some form of low resistivity patterns in the drainage corridor; underlain by a low resistive layer $<150 \Omega.m$, the drop in resistivity value could be associated with an increase in the amount of water content as revealed by MRS parameter, and finally a deeper thick layer up to depth of investigation with increased resistivity value $>200 \Omega.m$ which could be explained by some form of consolidated sediment and low MRS water content. The mountainous component is not fully characterized because it is severely undersampled. Therefore, some fictitious profiles have been added by taking the reference to ERT Line 7 conducted in the northwest of the study area near the drainage corridor. Thus, two depth-wise layers can be sorted; a thin surficial layer with low electrical resistivity $<150 \Omega.m$ spanning over the relief valley, followed by a layer with highly developed electrical resistivity up to the depth of investigation with some high spot reaching about $1500 \Omega.m$ in the northwest of Figure 26. But it also shows the sharp boundary between low and high resistivity value at model's northwest bottom, which can be associated to the weakness of interpolation algorithm and also can be associated to averaging effect because the model cells are far away from the sampled point.

6.3.2. Insight into subsurface hydrogeological setting based on MRS outputs

6.3.2.1 Interpretation of MRS hydrogeological layers

In natural geological formations, hydrogeological properties are highly heterogeneous in space at all scales. Mapping of hydrogeological layers and associated properties has been based on a classic way of gathering information from boreholes data and associated aquifer test to get insights into the subsurface hydrogeological structure. As mentioned earlier, in section 3, hydrogeophysical methods have gained particular attention for hydrogeological system parameterization because they provide an efficient way of estimating hydrogeological parameters and aquifer geometry. The integral application of hydrogeophysical methods has been historically performed to provide supporting information for subsurface hydrogeological system parameterization (e.g., Chaudhuri et al. 2013; Francés et al.2014). In spite of their capabilities, the overall spatial resolution provided by hydrogeophysical methods is much coarser than depth-wise geometry due to an unoptimized number of field measurement even at a small catchment scale. Thus, the combination of hydrogeophysical profiles and geostatistical tools can provide useful information on the extent of hydrogeological layers. Moreover, geostatistical tools were also developed for analysis, visualization, and modeling of hydrogeological properties (Chaudhuri et al. 2013). Lubczynski and Roy 2003, 2007). It is suggested that the combination of MRS signal amplitude (an indication of water content) and decay time constant (an indication of water extractability) can be used to analyze inverted MRS geophysical curves and define hydrogeological layers, linking different MRS profiles.

In this work, MRS hydrogeological layers of the study area were defined by interpreting MRS outputs. After defining MRS hydrogeological layers for each sounding, RockWorks was used to interpolate layers linking MRS profiles. The model extent was constrained by the maximum and minimum coordinates of the field measurement. Furthermore, additional fictitious profiles were defined by schematizing the study

area into three components: (i) A component with topographic relief which acts as water collector ;(ii) A drainage corridor mostly running from west to east of the study area which includes in its periphery the following field measurement: MRS10-1; MRS6-1; MRS 5-2; ERT Line 4; and ERT line 7, and (iii) A plain component composed by alluvial deposits with storage role

The combined interpretation of the vertical distribution of MRS free water content (Θ_{MRS}) and decay time constant (T_2^*) was enabled to define MRS depth-wise hydrogeological layers. This approach has been successfully applied by Francés et al. (2014) to provide supporting information for constraining aquifer geometry . The MRS hydrogeological layers have been defined in two steps:

- i. Combined interpretation of MRS geophysical curves(Θ_{MRS} and T_2^*) to define layer thickness and associated hydrogeophysical properties.
- ii. Assigning lithological properties (petrophysical information) by considering the average value of decay time constant (T_2^*) using Table 4.

To interpret MRS hydrogeological layers, the MRS data set was divided into two groups to provide the link between MRS profiles: a group of plots with similar patterns as a function of depth and a group of plots with inconsistent patterns versus depth. But in general, all profiles have three depth-wise MRS hydrogeological layers. Thus, 10 out of 18 profiles present almost similar patterns (Appendices.) except some interruption for decay time constant (T_2^*) at MRS5-1, MRS5-2 and, MRS7-1, MRS8-2 for deep and top layer, respectively. Thus, three depth-wise layers can be sorted: a surficial thin layer characterized by low MRS water content with weighted average ranging from $\sim 0.14\%$ to 6.38% and thickness extending from 0.5m to 17.7m, but with an outlier of 77.1m at MRS9-2, underlain by a thick layer with varying thickness of 9.4 m to 138.8m at MRS5-2 and MRS7-2 for minimum and maximum respectively , being characterized by high MRS water content with weighted average ranging from $\sim 10\%$ to 41% at MRS5-2 and MRS8-2 for minimum and maximum value, respectively, and finally a deeper layer with varying depths extending from 28m deep at MRS5-2 up to the depth of investigation being characterized by the low weighted average of Θ_{MRS} ranging from $\sim 0\%$ to 7.8% and high developed decay time constant (See Table 12).

Table 12. MRS hydrogeological layer for plots with similar patterns versus depth. Spatial distribution of MRS field measurement can be found in Figure 28

ID	Depth(m)		Thickness (m)	Decay time(T2*)			water content(%)			MRS Layers	Petropysical information
	Top	Bottom		Max	Min	Average	Max	Min	Average		
MRS1-1	0	5.25	5.25	332.70	30.00	181.34	4.63	0.43	4.1	Layer1	Clayey Sands or Very fine Sands
MRS1-1	5.25	82	76.75	84.83	68.00	77.80	16.99	9.32	12.2	Layer2	Fine Sands
MRS1-1	82	225	143	353.84	238.48	296.16	2.07	0.40	1.1	Layer3	Coarse and gravely sands
MRS2-1	0	11.87	11.87	106.28	30.00	55.41	6.33	0.72	5.0	Layer1	Clayey Sands or Very fine Sands
MRS2-1	11.87	54.93	43.06	77.31	51.92	64.61	14.15	11.75	12.7	Layer2	Fine Sands
MRS2-1	54.93	225	170.07	100.00	99.91	99.97	4.97	0.27	1.7	Layer3	Fine Sands
MRS3-1	0	11.87	11.87	66.19	0.00	32.06	5.75	0.00	4.1	Layer1	Clayey Sands or Very fine Sands
MRS3-1	11.87	94.92	83.05	122.50	53.58	91.23	21.92	12.21	16.2	Layer2	Fine Sands
MRS3-1	94.92	225	130.08	1000.00	1000.00	1000.00	3.95	0.93	2.2	Layer3	Less Weathered Rock
MRS3-2	0	3.52	3.52	67.28	36.32	51.80	2.49	0.62	2.2	Layer1	Clayey Sands or Very fine Sands
MRS3-2	3.52	94.92	91.4	119.33	40.13	80.00	18.84	8.33	13.3	Layer2	Fine Sands
MRS3-2	94.92	225	130.08	1000.00	652.49	826.70	1.69	0.38	0.9	Layer3	Less Weathered Rock
MRS4-1	0	8.33	8.33	30.00	0.00	15.00	1.13	0.00	0.1	Layer1	Clayey Sands or Very fine Sands
MRS4-1	8.33	130.21	121.88	151.94	64.51	106.97	16.53	8.52	11.3	Layer2	Fine Sands
MRS4-1	130.21	225	94.79	453.89	453.89	453.80	1.01	1.01	1.0	Layer3	Coarse and gravely sands
MRS7-1	0	8.33	8.33	231.72	30.00	80.43	3.73	1.88	2.7	Layer1	Clayey Sands or Very fine Sands
MRS7-1	8.33	130.21	121.88	278.06	71.54	158.89	33.31	16.59	20.4	Layer2	Fine sands
MRS7-1	130.21	225	94.79	1000.00	1000.00	1000.00	4.32	1.63	2.8	Layer3	Less Weathered Rock
MRS7-2	0	11.87	11.87	115.06	30.00	58.35	7.26	3.10	6.4	Layer1	Clayey Sands or Very fine Sands
MRS7-2	11.87	150.73	138.86	343.51	130.60	172.66	26.53	11.18	18.8	Layer2	Fine sands
MRS7-2	150.73	225	74.27	943.58	943.58	943.58	3.18	3.18	3.2	Layer3	Less Weathered Rock
MRS8-2	0	17.71	17.71	0.00	0.00	0.00	0.00	0.00	3.2	Layer1	Coarse and gravely sands
MRS8-2	17.71	41.98	24.27	149.13	34.41	91.77	41.87	41.87	41.9	Layer2	Fine Sands
MRS8-2	41.98	225	183.02	1000.00	0.00	421.42	9.88	0.00	4.3	Layer3	Gravels
MRS5-1	0	1	1	1000.00	30.00	353.10	8.36	0.65	0.7	Layer1	Clayey Sands or Very fine Sands
MRS5-1	1	41.98	40.98	414.25	43.18	159.60	33.02	9.28	22.2	Layer2	Fine sands
MRS5-1	41.98	225	183.02	0.00	0.00	0.00	0.00	0.00	0.0	Layer3	Fine sands
MRS5-2	0	8.33	8.33	30.00	0.00	15.00	1.49	0.00	0.2	Layer1	Sand Clayey
MRS5-2	8.33	28.13	19.8	184.76	184.76	184.76	10.43	10.43	10.4	Layer2	Coarse and gravely sands
MRS5-2	28.13	225	196.87	694.53	167.64	354.80	7.99	1.57	7.9	Layer3	Coarse and gravely sands

For plots with inconsistent patterns as a function of depth are presented in Appendices. However, for each sounding three depth-wise MRS hydrogeological layers can be sorted but with inconsistent patterns between MRS water content and decay time, except for MRS10-1 which present only two layers. Thus three depth-wise layers are interpreted as follows; a thin surficial layer with MRS thickness of 0.5m to 17.7m for minimum and maximum respectively but with an outlier of 77.17m at MRS9-2, this layer is characterized by low Θ_{MRS} varies between $\sim 2.19\%$ to 6.8% ; underlain by a thick layer with a thickness of 9.49m to 94.42m, being characterized by a high weighted average of Θ_{MRS} ranging from $\sim 8.5\%$ to 17.7% ; and finally a deeper layer with a thickness extending from 8.33m deep at MRS10-1 to MRS maximum resolution depth, characterized by low Θ_{MRS} varies between $\sim 0\%$ to 7.9% (See Table13).

Table13. MRS hydrogeological layer for plots with inconsistent Patterns versus depth. Spatial distribution of MRS field measurement can be found in Figure 28.

ID	Depth(m)		Thickness(m)	Decay time(T_2^*)			water content(%)			MRS Layers	Petrophysical information
	Top	Bottom		Max	Min	Average	Max	Min	Average		
MRS8-1	0	5.25	5.25	45.69	30.00	37.84	3.11	0.65	2.8	Layer1	Clayey Sands or Very fine Sands
MRS8-1	5.25	82	76.75	107.58	88.23	96.61	16.39	8.08	10.7	Layer2	Fine Sands
MRS8-1	82	225	143	41.68	39.96	40.80	4.03	0.78	2.1	Layer3	Clayey Sands or Very fine Sands
MRS11-1	0	17.71	17.71	1000.00	1000.00	1000.00	0.43	0.27	5.0	Layer1	Coarse and gravely sands
MRS11-1	17.71	82	64.29	77.05	69.99	73.50	18.15	8.63	12.2	Layer2	Fine Sands
MRS11-1	82	225	143	886.81	218.86	552.80	1.45	0.27	0.8	Layer3	Gravels
MRS11-2	0	0.5	0.5	74.50	74.50	74.50	4.57	4.57	4.6	Layer1	Fine Sands
MRS11-2	0.5	57.98	57.48	1000.00	74.92	288.13	36.23	2.29	17.7	Layer2	Coarse and gravely sands
MRS11-2	57.98	225	167.02	0.00	0.00	0.00	0.00	0.00	0.0	Layer3	Coarse and gravely sands
MRS9-2	0	77.17	77.17	299.42	249.74	230.00	11.06	6.77	6.9	Layer1	Coarse and gravely sands
MRS9-2	77.17	164.02	86.85	69.50	69.30	69.40	20.30	15.70	17.7	Layer2	Fine Sands
MRS9-2	164.02	225	60.98	1000.00	79.70	79.70	20.33	7.01	7.9	Layer3	Fine sands
MRS9-1	0	0.5	0.5	191.86	191.86	191.86	2.53	2.53	2.5	Layer1	Coarse and gravely sands
MRS9-1	0.5	94.92	94.42	154.02	93.27	114.50	24.78	11.79	16.7	Layer2	Fine Sands
MRS9-1	94.92	225	130.08	115.65	115.65	115.65	1.92	1.92	4.1	Layer3	Fine Sands
MRS4-2	0	14.4	14.4	257.03	119.79	188.50	6.43	1.16	5.8	Layer1	Coarse and gravely sands
MRS4-2	14.4	48.6	34.2	90.83	90.83	90.83	8.56	8.56	8.6	Layer2	Fine Sands
MRS4-2	48.6	225	176.4	1000.00	69.23	534.60	5.88	0.70	2.7	Layer3	Coarse and gravely sands
MRS6-1	0	1.35	1.35	1000.00	1000.00	1000.00	2.75	1.25	2.2	Layer1	Gravels
MRS6-1	1.35	10.82	9.47	338.31	126.14	232.20	15.24	9.85	13.4	Layer2	Coarse and gravely sands
MRS6-1	10.82	225	214.18	1000.00	30.12	619.40	6.64	0.08	1.1	Layer3	Less weathered Rock
MRS10-1	0	8.33	8.33	594.41	429.81	512.00	7.13	2.06	6.5	Layer1	Gravels
MRS10-1	8.33	225	216.67	1000.00	178.66	746.70	3.99	0.47	1.7	Layer3	Less weathered Rock

After defining MRS hydrogeological layers, associated lithology was assigned based on decay time constant value (T_2^*) referring to Table 4, except for some profiles which represent a deeper layer with higher developed T_2^* (not part of Table 4). Nevertheless, these layers were interpreted as a less weathered rock with low storage. To define the spatial extent of interpreted MRS hydrogeological layers, the database was created by transforming MRS hydrogeological layers into an appropriate format, which complies with the modeling software.

The MRS field measurement coordinates were converted into UTM meter coordinates (WGS84 System, UTM Zone 47N) to define project dimensions using Rockworks borehole Manager. Thus, it was necessary for the coordinate system to be consistently applied to ensure proportionality in the field measurement locations and additional fictitious profiles. Rockworks stratigraphy tool was used to interpolate layers linking MRS hydrogeological profiles. To ensure stratigraphy type is entered correctly, Rockworks stratigraphy type table was used to assign a unique code for each MRS hydrogeological layers as defined in Table 12 and Table13.

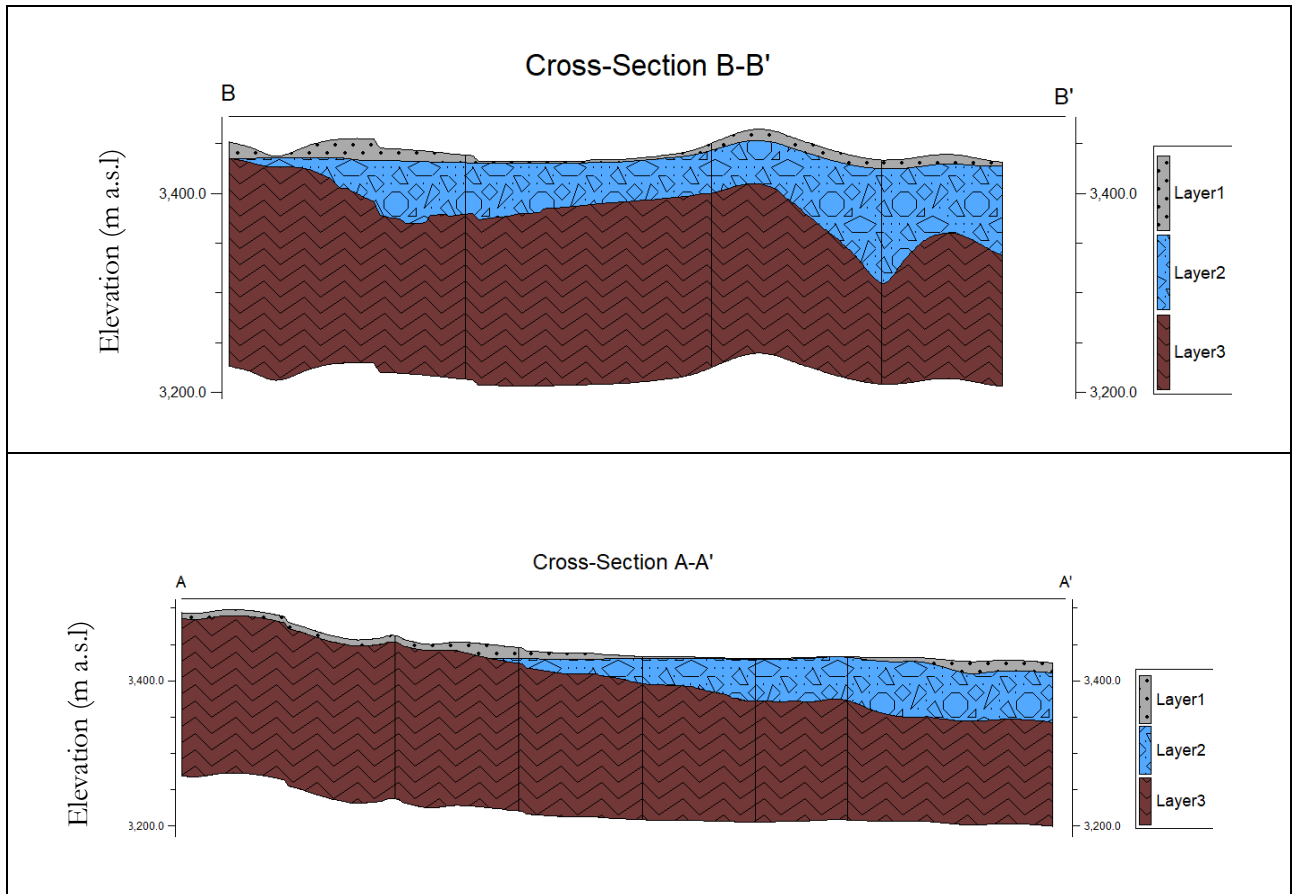


Figure 27 .Cross section of MRS hydrogeological layers and field plan location is depicted figure 28

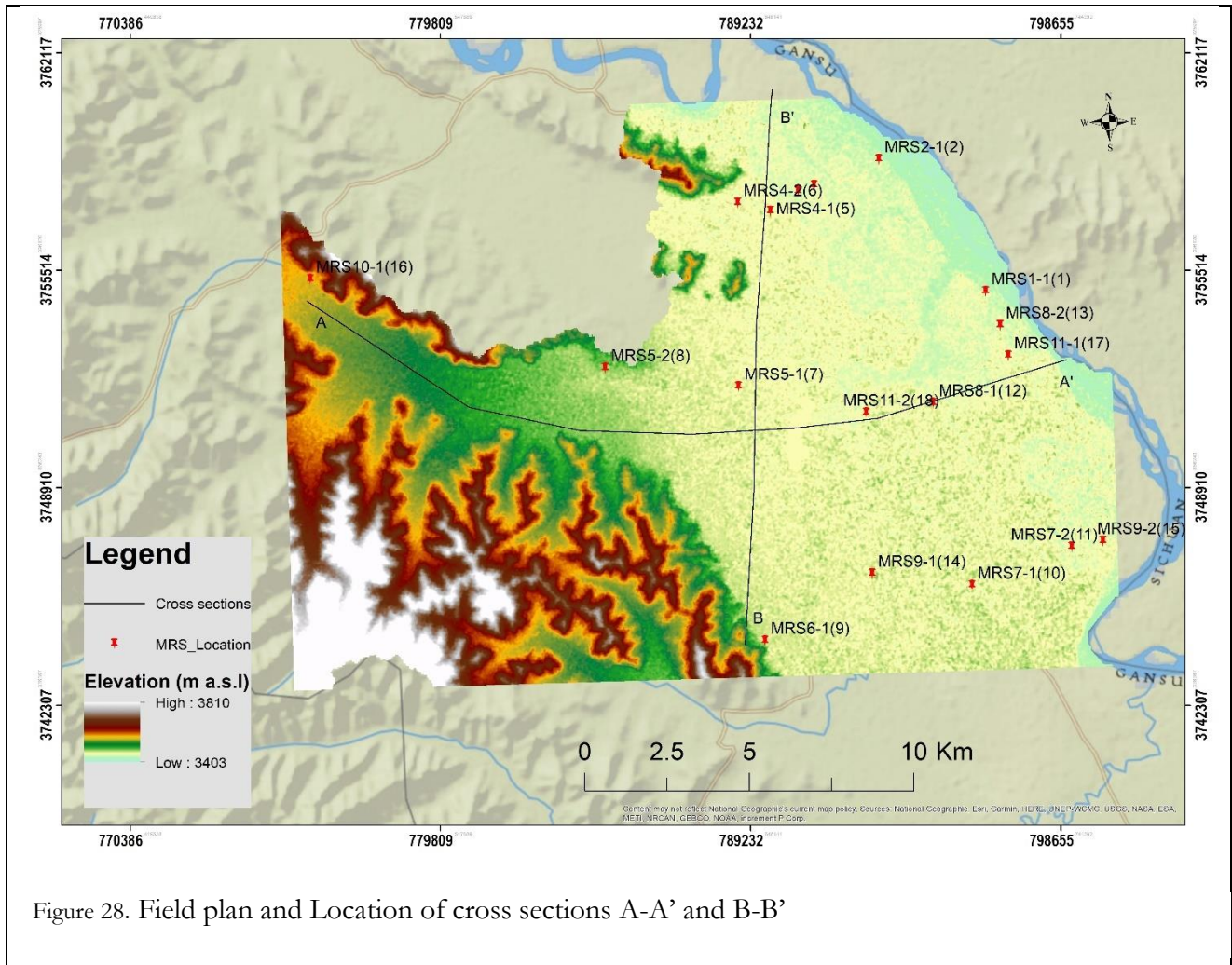


Figure 28. Field plan and Location of cross sections A-A' and B-B'

6.3.2.2 3-D Lithological model based on MRS outputs

Creating a lithology model can take some time depending on model resolution or details of the data available. Therefore, to develop a lithological model of the study area the model vertical resolution was assigned based on the minimum depth of MRS hydrogeological layer to make each interpreted unit visible in the 3D model and lateral resolution was selected by considering the resolution of Digital Elevation Model (DEM). Therefore, 30X30m and 0.5m for the horizontal and vertical resolution were used respectively. The model was constrained by the shapefile of the study area defined by maximum and minimum coordinates of field measurement, DEM was also applied to constrain the model to ground surface elevation, and the model subsurface depth was restricted to the depth of investigation. Once the database and model settings entered correctly, the MRS lithological model was constructed using the interpolation algorithm available in RockWorks. Four different interpolation algorithms are available for modeling lithology (i.e., Lateral Blending, Lateral extrusion, Closest distance point, and Highest probability). However, the choice of the best interpolation technique which reflect the geometry of geological boundaries is a difficult task.

Therefore, lateral blending was selected to interpolate MRS lithological unit (petrophysical information) as depicted in Table 12 and Table13, because it is reported to be particularly useful for horizontally contiguous data, which are in good agreement with MRS lithological layers of the study area.

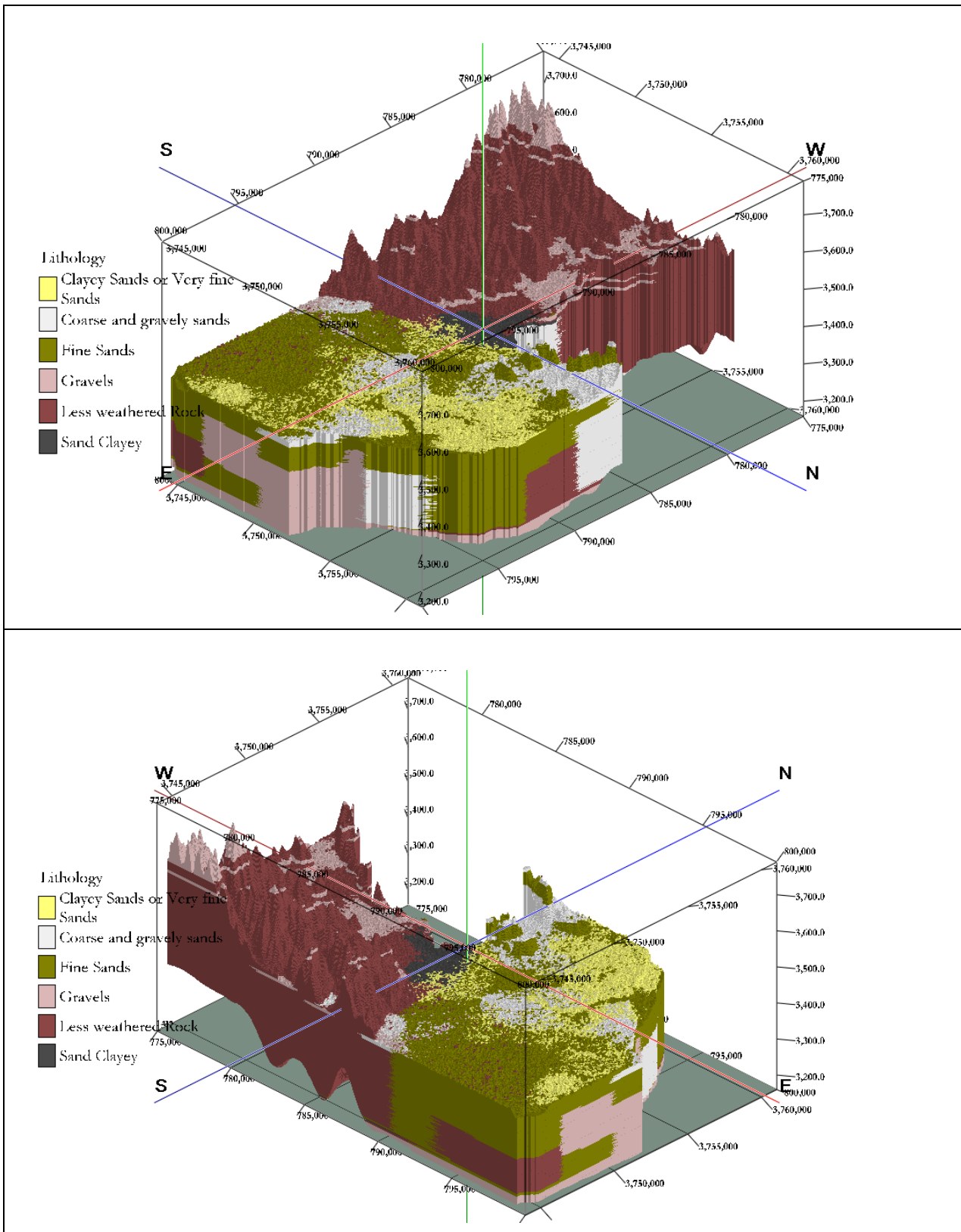


Figure 29.3-D MRS Lithological model of the study area. Vertical exaggeration is 20.

6.3.2.3 Hydrogeological parameterization with MRS.

The conventional way of estimating aquifer hydraulic parameters (both storage and flow) is through the analysis of data from borehole drilling and associated aquifer test. However, this method is expensive and time-consuming, and data interpretation is associated with certain error. Thus, the complementary approach of using Magnetic Resonance Sounding and aquifer pumping test at the same site showed the ability to improve aquifer characterization compared to the classic way. The capability of MRS to characterize subsurface hydrogeological parameters is currently limited to saturated zone because of the current development of MRS instrumentation, which does not allow to detect fast decaying signal generated by capillary or bound water from vadose zone. Therefore, the calculated parameters reflect only the hydrogeological parameters of MRS saturated layer. The extent of the saturated layer (Layer 2 of Figure 27) was estimated using the combined interpretation of MRS geophysical curves (section 6.3.2.1), which fit well with the drop in electrical resistivity measured by ERT at each sounding. Therefore, this may reflect groundwater presence, and it was confirmed by the existing borehole (Figure 11) which is located near ERT line3 and MRS3-2 (See Figure 20) where the groundwater table is reported to be at 12m below ground surface.

In this work, the hydraulic parameters of the saturated layer were estimated by adopting the methodology and calibration coefficient used for other sites but with similar lithological properties. For instance, the flow parameters were calculated by using calibration coefficients estimated from aquifer with similar lithological properties to our study area. The storage parameter (Specific yield) was assessed using a diagram relating MRS water content and specific yield, as a function of the median of grain size for aquifer composed mainly of fine sands. It is worthwhile to say that this method is likely depending on the geological context.

Flow parameters

The MRS hydraulic transmissivity and conductivity were estimated using Equation 10 and Equation 12 respectively. The calibration coefficient of $0.9\text{E-}09 \text{ m}\cdot\text{s}^{-3}$ (see Table 5) assigned in fine sand with clay in Doñana aquifer (Plata & Rubio, 2008) was adopted because the saturated layer of our study area is mostly composed by fine sand as shown in Figure 29. The calculated hydraulic conductivity varies between $7.00\text{E-}06 \text{ m}\cdot\text{s}^{-1}$ to $1.94\text{E-}05 \text{ m}\cdot\text{s}^{-1}$ and $4.8\text{E-}07 \text{ m}\cdot\text{s}^{-1}$ to $1.3\text{E-}05 \text{ m}\cdot\text{s}^{-1}$ when using T_1 and T_2^* respectively (See Table 14). Transverse decay time (T_2^*) represent low values of flow parameters compared to longitudinal decay time (T_1), but it varies consistently with lithology type.

Storage parameter

The MRS specific yield of the saturated layer was estimated using the relationship between MRS water content and specific yield defined for aquifer with granulometry composed by fine sands in SW of Niger (see Figure 7). This relationship is built on the fact that the amount of undetectable water by MRS is primary depending on the mean relaxation time (T_2^*), which is also depending on pore size. The estimated value of specific yield ranges from 1.5% to 32% with an overall average of 5.4% and the values of specific yield at each sounding are presented in Table 14.

Table 14. Parameterization of MRS saturated layer (Layer2) using constant calibration coefficient (C_T): (a) longitudinal decay time constant (T_1) and (b) Using transverse decay time (T_2^*); S_y - Specific yield, θ_{MRS} -MRS free water Content; T_{MRS}, K_{MRS} -MRS estimates of Transmissivity and Hydraulic conductivity.

ID	Depth(m)		Thickness(m)	T1(ms)	$\theta_{MRS}(\%)$		$S_y(\%)$	C_T m.s ⁻³	T_{MRS} m ² .s ⁻¹	K_{MRS} ms ⁻¹	K_{MRS} m.d ⁻¹	Lithology
	Top	Bottom			Weighted average							
MRS1-1	5.25	82	76.75	291.3	12.24	2.4	9E-10	7.17E-04	9.34E-06	0.8	Fine Sands	
MRS2-1	11.87	54.93	43.06	325.04	12.65	2.6	9E-10	5.18E-04	1.20E-05	1.0	Fine Sands	
MRS3-1	11.87	94.92	83.05	301.8	16.22	3.8	9E-10	1.10E-03	1.33E-05	1.1	Fine Sands	
MRS3-2	3.52	94.92	91.4	328.3	13.27	2.8	9E-10	1.18E-03	1.29E-05	1.1	Fine Sands	
MRS4-1	8.33	130.21	121.88	296.1	11.28	2.0	9E-10	1.09E-03	8.90E-06	0.8	Fine Sands	
MRS7-1	8.33	130.21	121.88	309	20.38	7.5	9E-10	2.13E-03	1.75E-05	1.5	Fine sands	
MRS7-2	11.87	150.73	138.86	222.91	18.79	5.9	9E-10	1.17E-03	8.40E-06	0.7	Fine sands	
MRS8-1	5.25	82	76.75	272.45	10.74	1.9	9E-10	5.51E-04	7.17E-06	0.6	Fine Sands	
MRS8-2	17.71	41.98	24.27	189.2	41.87	32.0	9E-10	3.27E-04	1.35E-05	1.2	Fine Sands	
MRS11-1	17.71	82	64.29	252.2	12.22	2.4	9E-10	4.50E-04	7.00E-06	0.6	Fine Sands Coarse and	
MRS11-2	0.5	57.98	57.48	238.2	17.75	6.9	9E-10	5.21E-04	9.06E-06	0.8	gravely sands	
MRS5-1	2.21	41.98	39.77	311.3	22.23	7.8	9E-10	7.71E-04	1.94E-05	1.7	Fine sands Coarse and	
MRS5-2	8.33	28.13	19.8	335.6	10.43	1.7	9E-10	2.09E-04	1.06E-05	0.9	gravely sands	
MRS9-2	77.17	164.02	86.85	238.17	17.73	5.1	9E-10	7.86E-04	9.05E-06	0.8	Gravels	
MRS9-1	0.5	94.92	94.42	278.26	16.54	3.9	9E-10	1.09E-03	1.15E-05	1.0	Fine Sands	
MRS4-2	14.4	48.6	34.2	340.9	8.56	1.5	9E-10	3.06E-04	8.96E-06	0.8	Fine Sands Coarse and	
MRS6-1	1.35	10.82	9.47	316.4	13.41	2.8	9E-10	1.14E-04	1.21E-05	1.0	gravely sands	

(a)

ID	Depth(m)		Thickness(m)	T2(ms)	$\theta_{MRS}(\%)$		$S_y(\%)$	C_T m.s ⁻³	T_{MRS} m ² .s ⁻¹	K_{MRS} ms ⁻¹	K_{MRS} m.d ⁻¹	Lithology
	Top	Bottom			Weighted average							
MRS1-1	5.25	82	76.75	77.8	12.2	2.4	9E-10	5.1E-05	6.7E-07	0.1	Fine Sands	
MRS2-1	11.87	54.93	43.06	64.61	12.7	2.6	9E-10	2.0E-05	4.8E-07	0.04	Fine Sands	
MRS3-1	11.87	94.92	83.05	91.23	16.2	3.8	9E-10	1.0E-04	1.2E-06	0.1	Fine Sands	
MRS3-2	3.52	94.92	91.4	80	13.3	2.8	9E-10	7.0E-05	7.6E-07	0.1	Fine Sands	
MRS4-1	8.33	130.21	121.88	106.97	11.3	2	9E-10	1.4E-04	1.2E-06	0.1	Fine Sands	
MRS7-1	8.33	130.21	121.88	158.89	20.4	7.5	9E-10	4.8E-04	3.9E-06	0.3	Fine sands	
MRS7-2	11.87	150.73	138.86	172.66	18.8	5.9	9E-10	7.0E-04	5.0E-06	0.4	Fine sands	
MRS8-1	5.25	82	76.75	96.61	10.7	1.9	9E-10	6.9E-05	9.0E-07	0.1	Fine Sands	
MRS8-2	17.71	41.98	24.27	91.77	41.9	32	9E-10	7.7E-05	3.2E-06	0.3	Fine Sands	
MRS11-1	17.71	82	64.29	73.5	12.2	2.4	9E-10	3.8E-05	5.9E-07	0.1	Fine Sands Coarse and	
MRS11-2	0.5	57.98	57.48	288.13	17.7	6.9	9E-10	7.6E-04	1.3E-05	1.1	gravely sands	
MRS5-1	2.21	41.98	39.77	159.6	22.2	7.8	9E-10	2.0E-04	5.1E-06	0.4	Fine sands Coarse and	
MRS5-2	8.33	28.13	19.8	184.756912	10.4	1.7	9E-10	6.3E-05	3.2E-06	0.3	gravely sands	
MRS9-2	77.17	164.02	86.85	69.4	17.7	5.1	9E-10	2.0E-03	2.3E-05	0.1	Fine Sands	
MRS9-1	0.5	94.92	94.42	114.5	16.5	3.9	9E-10	1.8E-04	2.0E-06	0.2	Fine Sands	
MRS4-2	14.4	48.6	34.2	90.830059	8.6	1.5	9E-10	2.2E-05	6.4E-07	0.1	Fine Sands Coarse and	
MRS6-1	1.35	10.82	9.47	232.2	13.4	2.8	9E-10	6.2E-05	6.5E-06	0.6	gravely sands	

(b)

6.3.3. Hydrogeophysical interpretation with applied geophysical methods

The study area was schematized into two main components; a component with topographic relief which acts as water collector and a plain component with storage capacity role. A plain component where all field measurements were conducted is characterized by alluvial deposits which are composed by conglomeratic silt with sand, gravel, and boulder with thickness varies between 50-60m of the Quaternary system (See Figure 2). The applied hydrogeophysical methods helped to estimate three depth-wise hydrogeophysical layers as depicted in figure 30 ; (i) a thin surficial layer with thickness varies between 0.5-17.7m and a mean thickness of 11.8m but with an outlier of 77.1m at MRS9-2 and this layer was interpreted as unsaturated zone with highly developed electrical resistivity $>200 \Omega.m$ and low MRS water content with an average of $\sim 3.6\%$, whose granulometry composed by very fine sands and sandy clay as revealed by MRS decay time constant (T_2^*) ; (ii) a layer with thickness ranging from 9.4m to 138.8m and a mean of 69.7m with less developed electrical resistivity $<150 \Omega.m$ and high average MRS water content $\sim 16.9\%$; and this layer was interpreted as saturated zone with soil materials composed of fine sands to coarse gravels as indicated by MRS decay time constant (T_2^*) ; (iii) and a thick deep layer with unknown thickness extending from minimum depth of 28.1m at MRS5-2 up to depth of investigation, being characterized by an increase of electrical resistivity $>150 \Omega.m$ and low MRS water content $\sim 2.49\%$. This layer was interpreted as less weathered rock with less porosity as indicated by MRS parameters and ERT resistivity value.

The topographic relief was interpreted as a water collector with less storage capacity. But, it was not fully characterized due to rugged relief, which does not allow implementation of the applied hydrogeophysical methods. However, the combined interpretation of hydrogeophysical profiles (MRS10-1 and ERT Lin7, see Figure 24) conducted in Northwest part of the study area helped to roughly estimate two depth-wise hydrogeophysical layers, mainly in the drainage corridor running from northwest to east ;. The top layer is a surficial thin layer with an average thickness of 8.3 m, with less developed electrical resistivity $<150 \Omega.m$ and moderate MRS water content $\sim 6.5\%$. This top layer was referred to as unsaturated zone with granulometry composed by gravels as indicated MRS decay time constant (T_2^*). The second layer is a thicker deep layer with a thickness extending from 8.3 m deep up the depth of investigation with highly developed electrical resistivity up to $1500 \Omega.m$ in the northerwest of the study area and a low average of MRS water content $\sim 1.5\%$. This layer was interpreted as an impervious zone with less porosity (Figure 30).

Table 15. Hydrogeophysical parameters for Maqu sub-catchment

Layer	depth(m)		Average thickness(m)	Θ_{MRS} Weighted average(%)		Resistivity($\Omega.m$)	hydrogeological interpretation	
	Min	Max		Min	Max		Rock Type	Zone
Layer1	0.5	17.7	11.8	0.14	6.9	$>200 \Omega.m$	Clayey sands and coarse gravels	Unsaturated zone
Layer2	0.5	164.5	69.7	8.5	41.8	$<150 \Omega.m$	Fine sand and gravels	Saturated zone
Layer3	8.3	225	145.9	0	7.8	$>150 \Omega.m$	Less weathered rock and mixture Coarse and gravely sands	Saturated zone with less storage

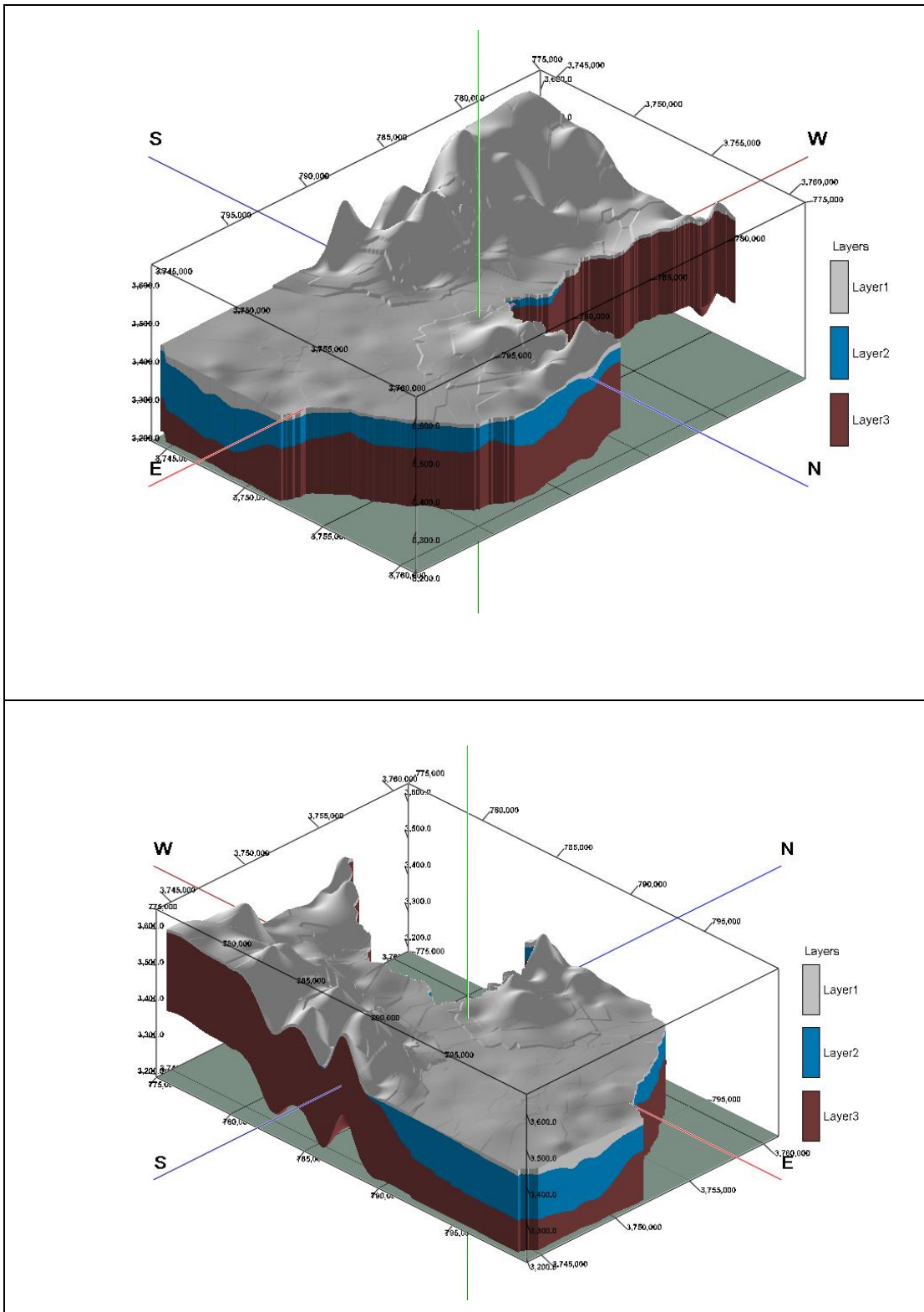


Figure 30. 3-D hydrogeophysical conceptual model

7. Conclusion and Recommendation

7.1. Conclusion

This study aimed to characterize subsurface hydrogeological setting, which influences groundwater occurrence in Maqu sub-catchment using hydrogeophysical methods. The hydrogeophysical data sets were acquired with two hydrogeophysical methods: Electrical Resistivity Tomography (ERT) and Magnetic Resonance Sounding (MRS). The integral interpretation of MRS hydrogeophysical curves (Θ_{MRS} and T_2^* versus depth) and supporting information from Electrical Resistivity Tomography profiles helped to classify hydrogeophysical layers and further interpolated using RockWorks,17 to establish their spatial extent over the study area.

The main conclusion from this study related to the applied hydrogeophysical methods are:

- The study area is characterized by two main hydrogeophysical components such as; topographic relief component which acts as a water collector and a plain component with storage capacity.
- Three depth-wise hydrogeophysical layers compose of the plain component; a thin surficial layer which is electrically resistive and with low MRS water content. The underlain layer is an electrically conductive layer with high MRS water content, and finally a deeper thick layer with developed electrical resistivity and low MRS water content.
- Two depth-wise hydrogeophysical layers compose of the topographic relief; a thin top electrically conductive layer with moderate MRS water content mainly in the valley relief. The second layer is a thick electrically resistive layer with low MRS water content.
- The MRS hydraulic conductivity varies between $0.6 - 1.7 \text{ m.d}^{-1}$ and $0.04 - 1.1 \text{ m.d}^{-1}$ when using longitudinal (T_1) and transverse (T_2^*) decay time constant, respectively. And the hydraulic conductivity estimated using T_2^* presents low average value of hydraulic conductivity compared to the value (T_1) but it varies consistently with lithology type.

7.2. Recommendations

For future hydrogeological studies, further development of the conceptual model is necessary to enhance our understanding on surface-groundwater interaction, and its influence on streamflow trends at the catchment scale. This work could be a step forward to gain further understanding of the subsurface hydrogeological setting. Mostly, it is recommended to conduct additional hydrogeophysical test for a different season to acquire various perspectives of hydrogeophysical properties. Even using a different type of hydrogeophysical methods, it is required to validate the acquired hydrogeophysical properties. For example, a test on groundwater salinity is essential because of its influences on ground electrical conductivity or borehole logging to control the variation of electrical resistivity during inverse modeling.

Lithological model of the study area was produced by considering a universal relationship between MRS decay time constant and lithological properties. Thus, this could lead to uncertainties over spatial extent of the lithological unit. Therefore, it is recommended to conduct a deep geological investigation to get insights into the subsurface geological setting.

MRS hydraulic parameters were estimated using the calibration coefficient and model adopted from literatures but with similar lithological properties to the study area. Despite having hydrogeological parameters values, which are in an acceptable range compared to the standard value, it is important to note that assigning single calibration coefficient to the entire aquifer or using a model established for other site is quite ambiguous, because no universal method has been proposed yet. Therefore, it is necessary to conduct an onsite hydrogeological investigation to evaluate MRS estimates.

List of references

- Baharuddin MFT, Hazreek ZAM, Azman MAA, Madun A (2018) Prediction of Groundwater Level at Slope Areas using Electrical Resistivity Method. *J Phys Conf Ser* 995:. doi: 10.1088/1742-6596/995/1/012084
- Baroncini-Turricchia G, Francés AP, Lubczynski MW, et al (2014) Integrating MRS data with hydrologic model - Carrizal Catchment (Spain). *Near Surf Geophys* 12:255–269. doi: 10.3997/1873-0604.2014003
- Baxter R, Hastings N, Law A, Glass EJ. (2008) Resistivity Characterization of 216-C-1, a-Complex, B-Plant, Purex, S-Complex, T-Plant, and 216-Z-16 Trench Project Sites. *Anim Genet* 39:561–563. doi: 10.13140/RG.2.2.23226.80328
- Bernard J, Legchenko A, Vermeersch F, et al (2006) PAPERS PRESENTED AT GEOPHYSICAL MEETINGS ON THE MAGNETIC RESONANCE SOUNDING METHOD: principles, equipment and case histories -
- Boucher M, Favreau G, Vouillamoz JM, et al (2009) Estimating specific yield and transmissivity with magnetic resonance sounding in an unconfined sandstone aquifer (Niger). *Hydrogeol J* 17:1805–1815. doi: 10.1007/s10040-009-0447-x
- Chaudhuri A, Sekhar M, Descloitres M, et al (2013) Constraining complex aquifer geometry with geophysics (2-D ERT and MRS measurements) for stochastic modelling of groundwater flow. *J Appl Geophys* 98:288–297. doi: 10.1016/j.jappgeo.2013.09.005
- Chirindja FJ, Dahlin T, Perttu N, et al (2016) Combined electrical resistivity tomography and magnetic resonance sounding investigation of the surface-water/groundwater interaction in the Urema Graben, Mozambique. *Hydrogeol J* 24:1583–1592. doi: 10.1007/s10040-016-1422-y
- Costabel S, Günther T (2014) Noninvasive Estimation of Water Retention Parameters by Observing the Capillary Fringe with Magnetic Resonance Sounding. *Vadose Zo J* 13:0. doi: 10.2136/vzj2013.09.0163
- Cuo L, Zhang Y, Zhu F, Liang L (2014) Characteristics and changes of streamflow on the Tibetan Plateau: A review. *J Hydrol Reg Stud* 2:49–68. doi: 10.1016/j.ejrh.2014.08.004
- Dahlin T (2001) The development of DC resistivity imaging techniques. *Comput Geosci* 27:1019–1029. doi: 10.1016/S0098-3004(00)00160-6
- Drouart E, Vouillamoz J-M (2005) Water, sanitation and hygiene for populations at risk, 2nd edn. Hermann, Editeurs des Sciences et des Arts, Paris
- Francés AP, Lubczynski MW, Roy J, et al (2014) Hydrogeophysics and remote sensing for the design of hydrogeological conceptual models in hard rocks - Sardón catchment (Spain). *J Appl Geophys* 110:63–81. doi: 10.1016/j.jappgeo.2014.08.015
- Giordano M, Zhu Z, Cai X, et al (2004) Water Management in the Yellow River Basin: Background, Current Critical Issues and Future Research Needs. Comprehensive Assessment Research Report 3. Colombo, Sri Lanka
- Guillen A, Calcagno P, Courrioux G, et al (2008) Geological modelling from field data and geological knowledge. Part II. Modelling validation using gravity and magnetic data inversion. *Phys Earth Planet Inter* 171:158–169. doi: 10.1016/j.pepi.2008.06.014
- Guo N, Li Y, Han L, Wang S (2012) The Effects of Climate Change on Different Types of Grassland in Maqu County in Northeast Tibetan Plateau. 1:1139–1142
- Hazreek ZAM, Faizal TBM, Aziman M, et al (2018) INTEGRAL APPLICATION OF ELECTRICAL RESISTIVITY TOMOGRAPHY, GEOCHEMISTRY AND BOREHOLE DATA IN GEOUNDWATER SEEPAGE ASSESSMENT. *Int J Civ Eng Technol* 9:8–19
- Hubbard S, Linde N (2011) Hydrogeophysics
- Lachassagne P, Baltassat J, Legchenko A, Gramont HM De (2005) The links between MRS parameters and the hydrogeological parameters. *Near Surf Geophys* 259–265
- Legchenko A, Baltassat JM, Beauce A, Bernard J (2002) Nuclear magnetic resonance as a geophysical tool for hydrogeologists. *J Appl Geophys* 50:21–46. doi: 10.1016/S0926-9851(02)00128-3
- Legchenko A, Comte JC, Ofterdinger U, et al (2017) Joint use of singular value decomposition and Monte-Carlo simulation for estimating uncertainty in surface NMR inversion. *J Appl Geophys* 144:28–36. doi: 10.1016/j.jappgeo.2017.06.010
- Legchenko A, Vouillamoz J-M, Roy J (2010) Application of the magnetic resonance sounding method to the

- investigation of aquifers in the presence of magnetic materials. *Geophysics* 75:L91–L100. doi: 10.1190/1.3494596
- Lekula M, Lubczynski M, Shemang EM (2017) Hydrogeological conceptual model of large and complex sedimentary aquifer systems – Central Kalahari Basin (Botswana) (under -review). *Hydrogeol J* 0–1. doi: 10.1016/j.pce.2018.05.006
- Ling C, Xu Q, Zhang Q, et al (2016) Application of electrical resistivity tomography for investigating the internal structure of a translational landslide and characterizing its groundwater circulation (Kualiangzi landslide, Southwest China). *J Appl Geophys* 131:154–162. doi: 10.1016/j.jappgeo.2016.06.003
- Liu C, Zheng H (2004) Changes in components of the hydrological cycle in the Yellow River basin during the second half of the 20th century. *Hydrol Process* 18:2337–2345. doi: 10.1002/hyp.5534
- Loke MH (2013) Tutorial : 2-D and 3-D electrical imaging surveys. *Geotomo Softw Malaysia* 127. doi: 10.1016/S0040-6090(99)00392-2
- Loke MH (2004) Tutorial: 2-D and 3-D Electrical Imaging Surveys, 2004 Revised Edition. 136
- Lubczynski M, Roy J (2005) MRS contribution to hydrogeological system parametrization. *Near Surf Geophys* 3:131–139. doi: 10.3997/1873-0604.2005009
- Lubczynski M, Roy J (2003) Hydrogeological interpretation and potential of the new magnetic resonance sounding (MRS) method. *J Hydrol* 283:19–40. doi: 10.1016/S0022-1694(03)00170-7
- Lubczynski M, Roy J (2004) Magnetic Resonance Sounding: New Method for Ground Water Assessment
- Lubczynski MW, Roy J (2007) Use of MRS for hydrogeological system parameterization and modeling. *Bol Geol y Min* 118:509–530
- Mathers SJ, Kessler H, Macdonald DMJ, et al (2012) The use of geological and hydrogeological models in environmental studies. Keyworth, Nottingham
- Mazzilli N, Boucher M, Chalikakis K, et al (2016) Contribution of magnetic resonance soundings for characterizing water storage in the unsaturated zone of karst aquifers. *GEOPHYSICS* 81:WB49-WB61. doi: 10.1190/geo2015-0411.1
- MICHELIS VT (1997) Some Principles , Methods and Devices for Surface Nuclear Magnetic Resonance (Snmr) and Logging Nmr. Andorra
- Natali M, Lidal EM, Viola I, Patel D (2013) Modeling terrains and subsurface geology. *Proc EuroGraphics 2013 State Art Reports* 155–173. doi: 10.2312/conf/EG2013/stars/155-173
- Pehme PE (2011) *Groundwater Geophysics: A Tool for Hydrogeology*, 2nd Ed. Springer Verlag Berlin Heidelberg, Berlin
- Plata JL, Rubio FM (2008) The use of MRS in the determination of hydraulic transmissivity: The case of alluvial aquifers. *J Appl Geophys* 66:128–139. doi: 10.1016/j.jappgeo.2008.04.001
- Prachi S, Adamane S (2015) COMPARATIVE STUDY OF RESISTIVITY SURVEY AND DOWSING METHOD TO LOCATE GROUNDWATER POTENTIAL. *Int J Sci Eng Technol Res* 4:1216–1221
- Raju NJ, Gossel W, Sudhakar M (2015) *Management of Water, Energy and Bio-Resources in the Era of climate change: Emerging Issues and Challenges*. Capital Publishing Company, New Delhi
- Roy J, Lubczynski MW (2014) Exploiting the MRS-phase information to enhance detection of masked deep aquifers: Examples from the Netherlands. *Near Surf Geophys* 12:309–324. doi: 10.3997/1873-0604.2013058
- Silvester PP, Ferrari RL (1996) Finite elements for electrical engineers. doi: 10.1017/CBO9781139170611
- Thorleifson LH, Berg RC, Russell HAJ (2007) Three-dimensional geologic mapping for groundwater applications: Workshop extended abstracts. *Minnesota Geol Surv Open File* 07-4:1–92. doi: 10.4095/221818
- Trabelsi F, Tarhouni J, Mammou A Ben, Ranieri G (2013) GIS-based subsurface databases and 3-D geological modeling as a tool for the set up of hydrogeological framework: Nabeul-Hammamet coastal aquifer case study (Northeast Tunisia). *Environ Earth Sci* 70:2087–2105. doi: 10.1007/s12665-011-1416-y
- UNESCO (2010) *Climate change and adaptation for water resources in Yellow River Basin, China*. Beijing, China
- Vouillamoz JM, Baltassat JM, Girard JF, et al (2007) Hydrogeological experience in the use of MRS. *Bol Geol y Min* 118:531–550
- Vouillamoz JM, Descloitres M, Toe G, Legchenko A (2009) Characterization of crystalline basement aquifers with MRS: comparison with boreholes and pumping tests data in Burkina Faso. *Near Surf Geophys* 3:205–213. doi: 10.3997/1873-0604.2005015
- Vouillamoz JM, Favreau G, Massuel S, et al (2008) Contribution of magnetic resonance sounding to aquifer characterization and recharge estimate in semiarid Niger. *J Appl Geophys* 64:99–108. doi: 10.1016/j.jappgeo.2007.12.006
- Vouillamoz JM, Lawson FMA, Yalo N, Descloitres M (2014) The use of magnetic resonance sounding for quantifying specific yield and transmissivity in hard rock aquifers: The example of Benin. *J Appl Geophys*

107:16–24. doi: 10.1016/j.jappgeo.2014.05.012

Vouillamoz JM, Sokheng S, Bruyere O, et al (2012) Towards a better estimate of storage properties of aquifer with magnetic resonance sounding. *J Hydrol* 458–459:51–58. doi: 10.1016/j.jhydrol.2012.06.044

Walsh DO, Grunewald ED, Turner P, et al (2014) Surface NMR instrumentation and methods for detecting and characterizing water in the vadose zone. *Near Surf Geophys* 12:271–284. doi: 10.3997/1873-0604.2013066

Wiese TC (2012) DC anisotropic resistivity sensitivity and inversion. University of Adelaide

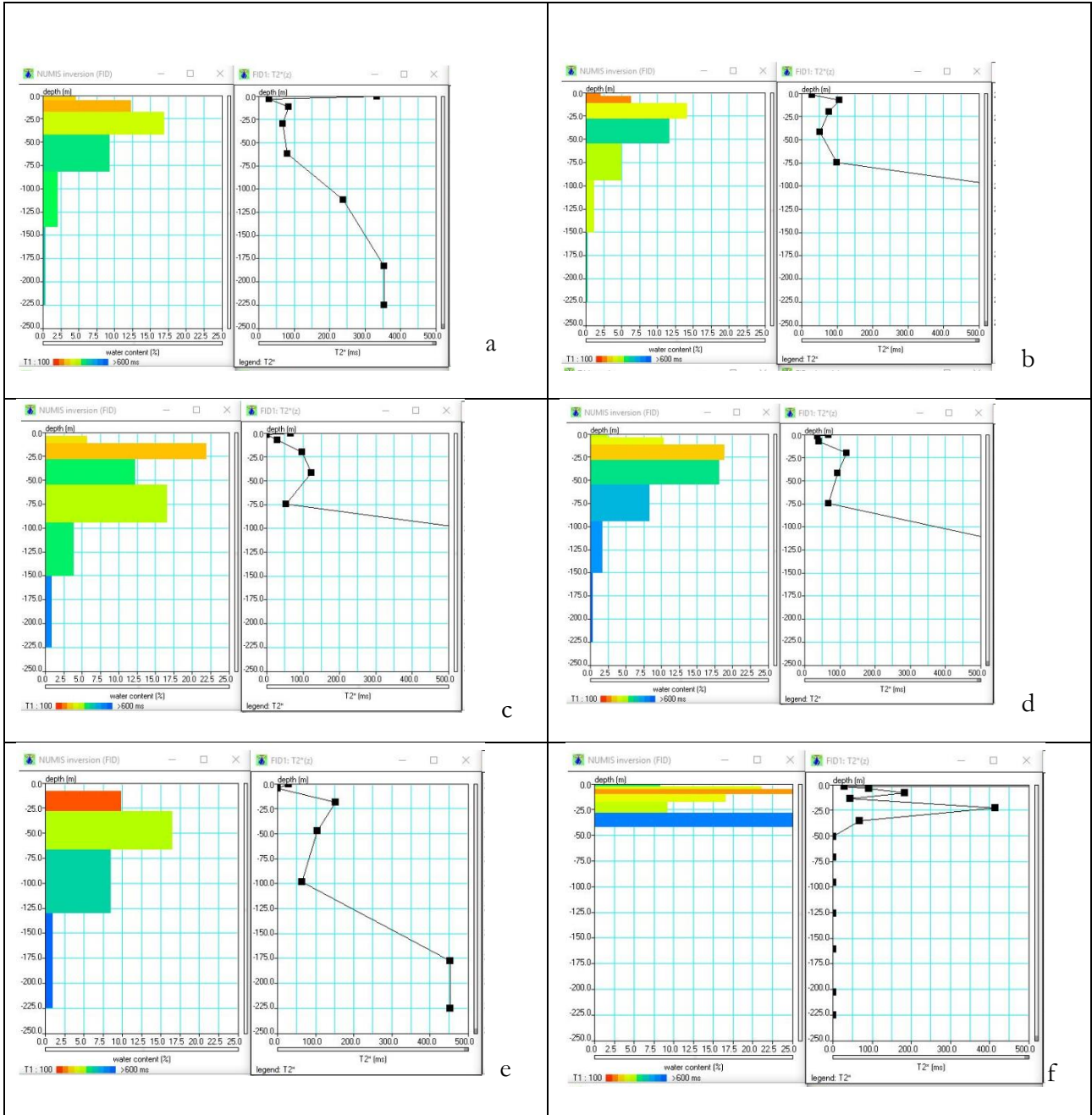
Yao Y, Zheng C, Liu J, et al (2015) Conceptual and numerical models for groundwater flow in an arid inland river basin. *Hydrol Process* 29:1480–1492. doi: 10.1002/hyp.10276

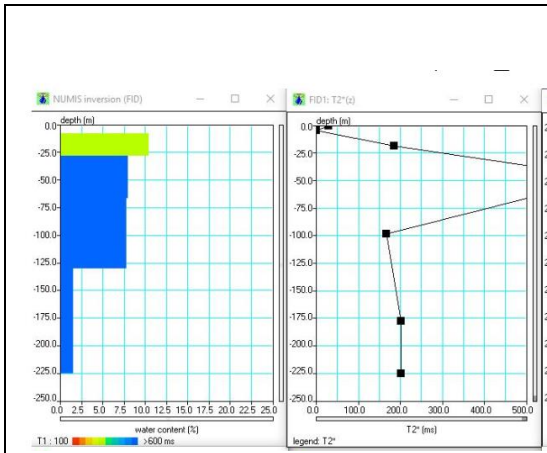
Zhang Y, Guo Y (2011) Water cycle changes during the past 50 years over the Tibetan Plateau : review and synthesis. In: *Cold Region Hydrology in a Changing Climate*. Melbourne, Australia

Zhou Y, Li W (2011) A review of regional groundwater flow modeling. *Geosci Front* 2:205–214. doi: 10.1016/j.gsf.2011.03.003

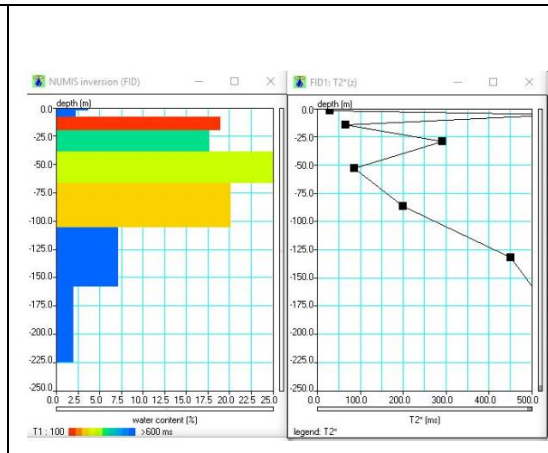
APPENDICES.

Appendix 1. MRS geophysical curves with similar patterns of Free water content (Θ_{MRS}) and decay time constant (T_2^*) as function of depth: MRS measurement location; (a) MRS1-1, (b) MRS2-1, (c) MRS3-1, (d) MRS3-2, (e) MRS4-1, (f) MRS5-1, (g) MRS5-2, (h) MRS 7-1, (i) MRS7-2, (j) MRS8-2.

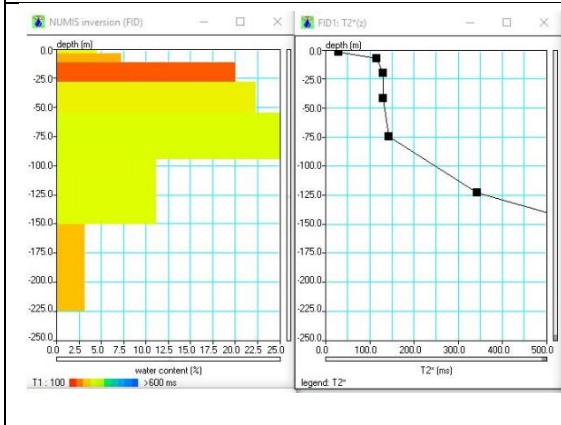




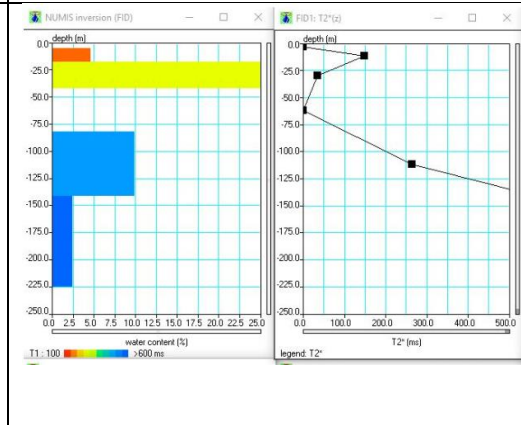
g



h

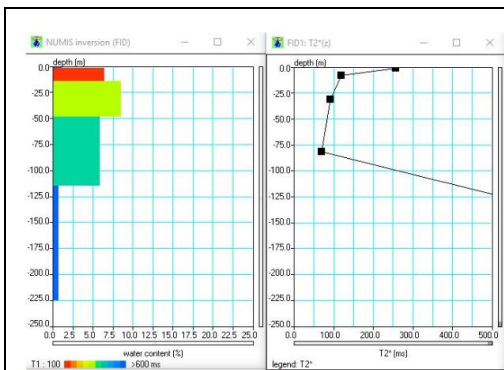


i

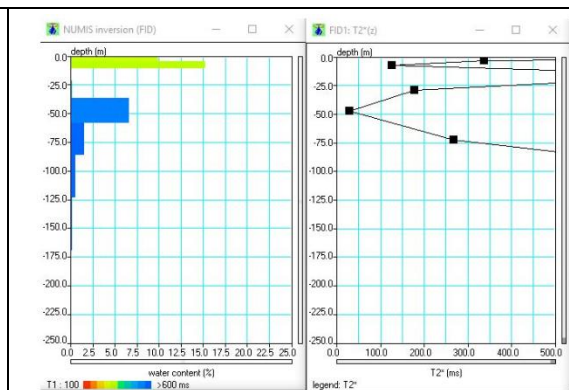


j

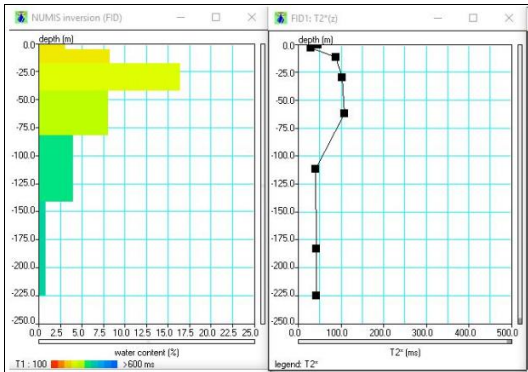
Appendix 2. MRS geophysical curves inconsistent patterns of Free water content (Θ_{MRS}) and decay time constant (T_2^*) versus depth: MRS measurement location; (a) MRS4-2, (b) MRS6-1, (c)MRS8-1, (d) MRS9-1, (e)MRS9-2, (f) MRS10-1,(g) MRS11-1, (h) MRS 11-2.



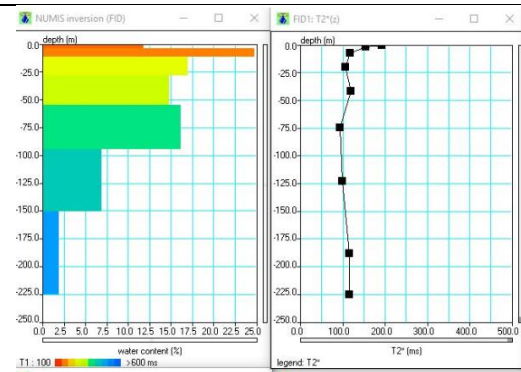
a



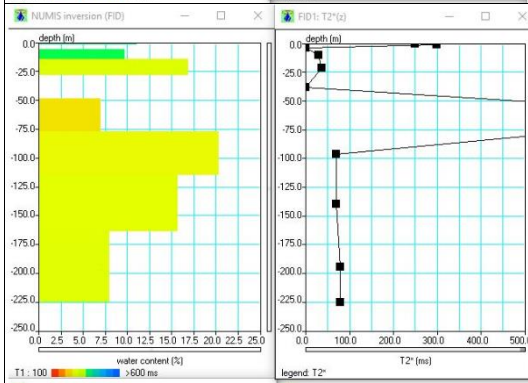
b



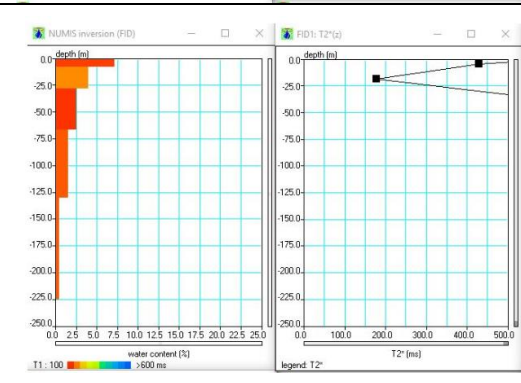
c



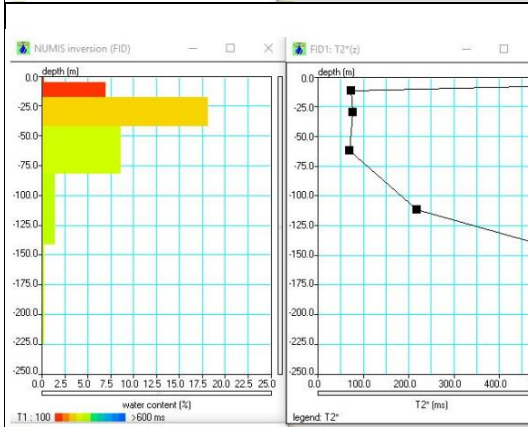
d



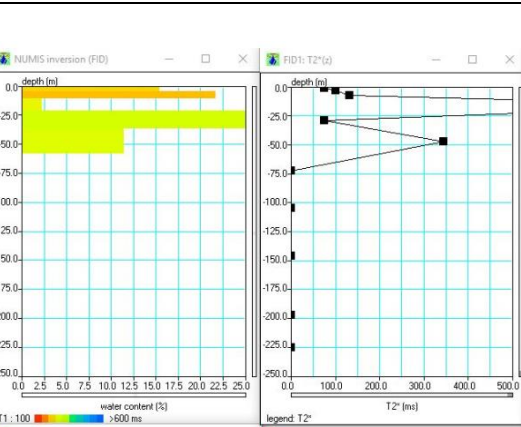
e



f



g



h